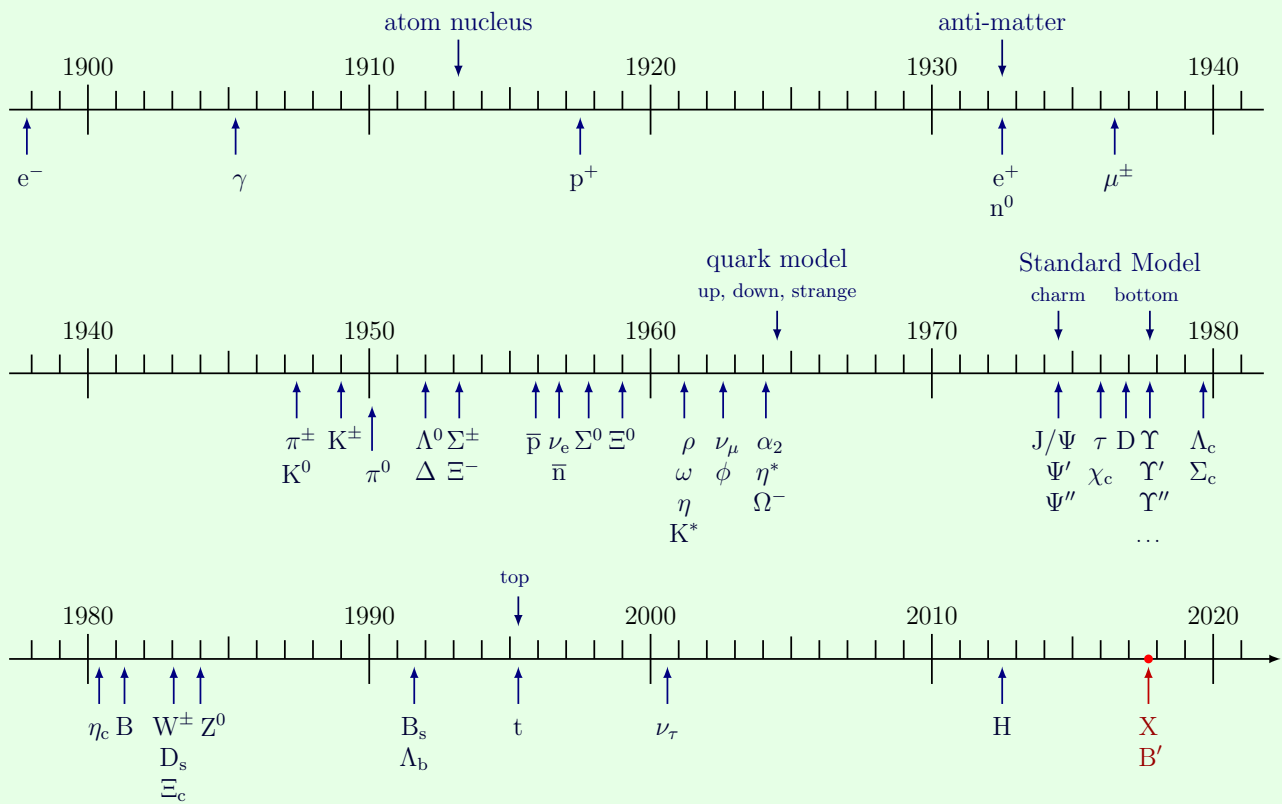

LECTURE NOTES OF SUBNUCLEAR PHYSICS

COLLECTION OF THE LECTURES NOTES OF PROFESSOR DONATELLA LUCCHESI.

EDITED BY

ARDINO ROCCO

ACADEMIC YEAR 2019-2020



Abstract

In this document I have tried to reorder the notes of the Subnuclear Physics course held by Professor Donatella Lucchesi at the Department of Physics of the University of Padua during the second semester of the 2019-20 academic year of the master's degree in Physics of Fundamental Interactions.

The notes are fully integrated with the material provided by the professor in the Moodle platform. In addition, I will integrate them, as best as possible, with the books recommended by the professor.

There may be formatting errors, wrong marks, missing exponents and even missing parts, since I'm still working on them. If you find errors or if you have any suggestions, let me know (ypu can send an e-mail at rocco.ardino@studenti.unipd.it, labeled with **SP::TYPO/SUGGESTION**) and I will correct/integrate them, so that this document can be a good study support. However, these notes are not to be intended as a substitute of the lectures held by the professor or of lecture notes made by other people.

Padova, Wednesday 15th April, 2020
Rocco Ardino

Contents

1	Introduction and Recap	3
1.1	Basic knowledge	3
1.2	Hydrogen atom and Positronium	5
1.3	Static Quark Model	9
1.3.1	Light quarks: charm and beauty	9
1.3.2	Light mesons	9
1.4	Leptons	11
2	Tools for calculations	13
2.1	Observables in experimental particle physics	13
2.2	Partial Width and Cross Section calculation	14
2.3	Phase Space integral calculation	15
3	Detectors for Particle Physics	19
3.1	Recap: interaction of particles with matter	19
3.1.1	Interactions involving the electrons and heavier particles	19
3.1.2	Interaction of photon with the matter	20
3.2	Gaseous, scintillator and solid state detectors	22
3.2.1	Gas detectors	22
3.2.2	Multiwire proportional chambers	24
3.2.3	Drift chambers	25
3.2.4	Semiconductor detectors	25
3.3	Track reconstruction	26
3.4	Calorimetry	27
3.4.1	Electromagnetic shower development	28
3.4.2	Hadronic shower development	28
3.4.3	Classification and response of calorimeters	30
3.4.4	Particle identification	32
4	Cross section of $e^+e^- \rightarrow \mu^+\mu^-$ and $e^+e^- \rightarrow hh$	33
4.1	Muon-Antimuon pair production: $e^+e^- \rightarrow \mu^+\mu^-$	33
4.1.1	Properties of massless spin- $\frac{1}{2}$ fermions	34
4.1.2	Matrix element and cross section evaluation	35
4.2	Hadron production: $e^+e^- \rightarrow \text{hadrons}$	36
5	Deep Inelastic Electron Scattering	39
5.1	The SLAC-MIT experiment	39
5.2	The parton model	40
5.3	Crossing symmetry	41
5.4	Cross section for electron-quark scattering	43
5.5	Bjorken scaling	45
6	Strong interactions	49

6.1	The gluon	49
6.1.1	Measurement of parton distribution functions	49
6.1.2	Photon emission in $e^+e^- \longrightarrow q\bar{q}$	51
6.1.3	Gluon effects on PDFs	52
7	Exercises	53
	Bibliography	55

Course structure and program

Informations

Suggested books:

- *Concepts of Elementary Particle Physics*, Michael E. Peskin.
It has a very good experimental approach, with theoretical concepts explained as well.
- Any other book where the same topics are presented is fine. For example, the book of Alessandro Bettini.

Exam modalities: the exam is slitted into two parts. These are:

- **Written exercises.**
The idea is to prepare two partial tests: one will take place almost at the middle of the course, one at the end. For each chapter of the reference book there are several exercises that are useful for the comprehension of the topics of the course.
- **Oral discussion.**
It will be focused on a single topic and it will take place after the written part.

The final evaluation will be a weighted mean of the two written exercises and of the oral discussion.

Remeber to subscribe to the Facebook group *Subnuclear Physics at DFA* for further informations and for infos on seminars of particle physics.

Course Program

- **Introduction and recap**
- **Tools for calculation.**
In order to understand all the following topics, we need some mathematical tools (that we already have but the way we are going to use them is different from the use we did in theoretical physics course). They are needed to evaluate the physical phenomena we are going to discuss.
- **Detectors for particle physics experiments.**
They are needed to perform measurements, so it is important to acquire a certain knowledge on them. For example, in order to choose why a detector is better than another one for a certain task and to set up a particle physics experiment. This part is not well described in the reference book, so we will use other books for this purpose.
- **Cross section of $e^+e^- \longrightarrow \mu^+\mu^-$ and $e^+e^- \longrightarrow hh$.**
The former is a very simple process and it is important for the study of many other processes. The ladder will be important to understand the basis of QCD.

Lecture 1.
Tuesday 10th
March, 2020.
Compiled:
Wednesday 15th
April, 2020.
Prof. Lucchesi

- **Strong interactions:**
 - ▷ **Deep inelastic scattering**
 - ▷ **Gluon**
 - ▷ **QCD**
 - ▷ **Partons and jets**
- **Electroweak interactions** (This part and the part on strong interactions sum up into the discussion on Standard Model):
 - ▷ **V-A Weak theory.**

It is the theory at the base of electroweak interaction, which we will build up.
 - ▷ **Gauge theory and symmetry breaking.**

This part will be discussed not so deeply since it was treated during the course of *Theoretical Physics of Fundamental Interactions*.
 - ▷ **W and Z^0 bosons.**

The most important items and measurements will be presented.
 - ▷ **Cabibbo theory and CKM.**

This part is needed in order to put the hadrons, in particular the quarks, into the electroweak theory. However, it will not be discussed deeply since it was presented during the bachelor course *Introduction to Nuclear and Subnuclear Physics*.
 - ▷ **CP violation, the B meson system.**

It will be a more experimental discussion.
- **New Physics** (we will try to give an answer to how we can go beyond the description given by Standard Model, in fact there are phenomena that are still not explained by this theory):
 - ▷ **Neutrino and Standard Model**
 - ▷ **Higgs properties**

Chapter 1

Introduction and Recap

1.1 Basic knowledge

Relativistic wave equations

Relativistic quantum field theory is necessary to describe quantitatively elementary particle interactions. Its description is not part of this course, so we will use it in simple cases and only when necessary.

It is assumed the following knowledge:

- Klein-Gordon equation (for boson fields):

$$\left(\frac{\partial^2}{\partial t^2} - \nabla^2 + m^2 \right) \psi(t, \vec{x}) = 0 \quad (1.1)$$

- Dirac equation (Klein-Gordon can't give a description for fermion fields):

$$\left(i\gamma_\mu \frac{\partial}{\partial x_\mu} - m \right) \psi(t, \vec{x}) = 0 \quad (1.2)$$

with $\psi = (\psi_1, \psi_2, \psi_3, \psi_4)$

- Basic concepts of fields and particles
- Basic concepts of Feynman diagrams

Natural Units

During the course we will use the natural units, therefore:

$$\hbar = c = 1 \quad (1.3)$$

Considering that:

$$\begin{aligned} 1 \text{ eV} &= 1.6 \cdot 10^{-19} \text{ J} \\ c &= 3 \cdot 10^8 \text{ m/s} \end{aligned}$$

we have:

$$1 \frac{\text{eV}}{c^2} = 1.78 \cdot 10^{-36} \text{ Kg}$$

Since $E^2 = p^2 c^2 + m^2 c^4$, it is convenient to measure p in GeV/c and m in GeV/c². For example the electron mass $m_e = 0.91 \cdot 10^{-27} \text{ g}$ corresponds to $m_e = 0.51 \text{ MeV}/c^2$. It is also useful to remember that $\hbar c = 197 \text{ MeVfm}$.

An interesting quantity to consider in natural units is the strength of the electric charge of the electron or proton. By taking into account the potential $V(r) = \frac{e^2}{4\pi\epsilon_0 r}$, the radius r in natural units has a dimension of Energy^{-1} . By this way it forces the following relation:

$$\alpha \equiv \frac{e^2}{4\pi\epsilon_0 \hbar c} = \frac{1}{137.036} \quad (1.4)$$

namely, the **fine structure constant**.

Symmetries

They are the corner stones of particle physics. The most important ones for our studies are the **space-time symmetries**, which can be classified into:

- Continuous symmetries:
 - ▷ Translation in time. The generator of the group of time translations is the operator H , namely the Hamiltonian, which is linked to the energy quantity.
 - ▷ Translation in space. The generator of the group of space translations is the operator \vec{p} , namely the momentum.
 - ▷ Rotations. In this case, the generator of the group of this kind of transformations is the angular momentum \vec{L} .

If a system is invariant under one of these transformations, the corresponding generator, so H , \vec{p} or \vec{L} , is conserved.

- Discrete symmetries:

- ▷ Parity P :

$$x^\mu = (x^0, \vec{x}) \xrightarrow{P} (x^0, -\vec{x}) \quad (1.5)$$

Fermions have half-integer spin and angular momentum conservation requires their production in pairs. We can define therefore just relative parity. By convention, the proton p has parity equal to $+1$. The parity of the other fermions is given in relation to the parity of the proton.

Parity of bosons can be defined without ambiguity since they are not necessarily produced in pairs.

Parity of a fermion and its antiparticle (i.e. an antifermion) are opposite, while parity of a boson and its anti-boson are equal.

Moreover, the parity of the positron is equal to -1 . Quarks have parity equal to $+1$, leptons have parity equal to $+1$. Their antiparticles have parity equal to -1 .

Lastly, parity of a photon is equal to -1 .

- ▷ Time Reversal T :

$$x^\mu = (x^0, \vec{x}) \xrightarrow{T} (-x^0, \vec{x}) \quad (1.6)$$

- ▷ Charge Conjugation C :

$$\text{Particle} \xleftrightarrow{C} \text{Antiparticle} \quad (1.7)$$

It is needed in order to restore a complete symmetry under the exchange of a particle with its antiparticle. A photon has -1 eigenvalue under C , which means: $C|\gamma\rangle = -|\gamma\rangle$.

Fermion-antifermion have opposite intrinsic parity and for non elementary particles the total angular momentum has to be considered, in fact the C parity goes like $(-1)^\ell$ or $(-1)^{\ell+1}$ (depending on the intrinsic parity).

Fundamental constituents of the matter

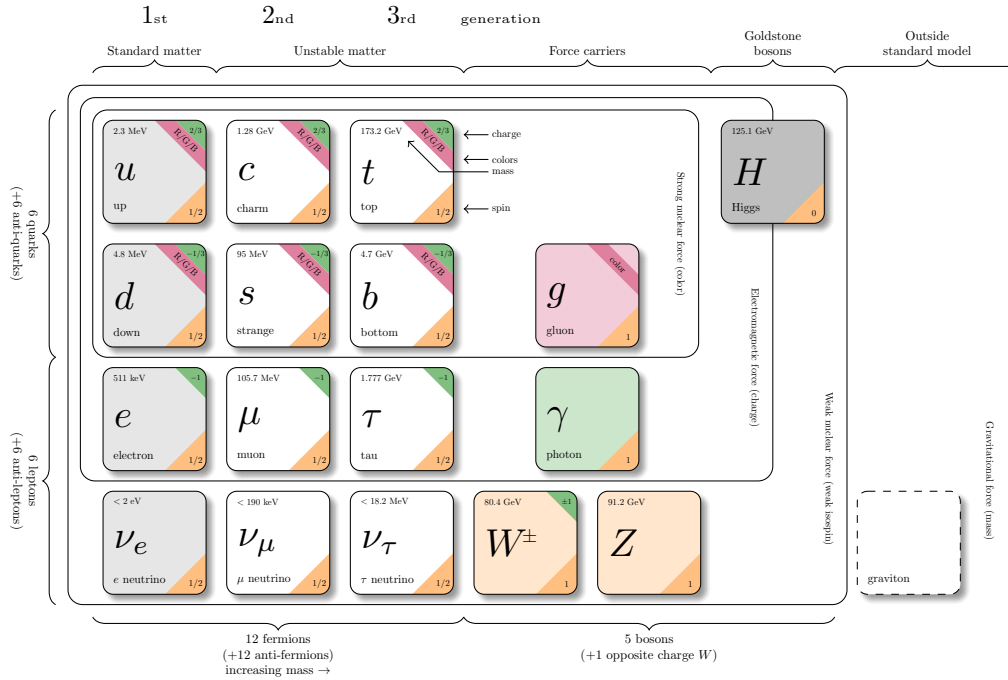


Figure 1.1: Standard Model particles.

1.2 Hydrogen atom and Positronium

We are going to study the already known system of the hydrogen atom, and compare it to the system of positronium. More in detail, our goal is to understand the e^+e^- bound state and the possible application of this model to the description of other systems. Therefore, we start from the hydrogen atom since it has some characteristics in common with the positronium.

In QM Physics, this bound state is really similar to the hydrogen atom. The assumptions for this one in the non relativistic limit are that the mass of the proton is much bigger than the mass of the electron ($m_p \gg m_e$) and the potential is given by:

$$V(r) = -\frac{e^2}{4\pi r} = -\frac{\alpha}{r} \quad (1.8)$$

From this potential, by solving the Schrödinger equation, we get the bound state energies:

$$E = -\frac{R_y}{n^2} \quad (1.9)$$

Lecture 2.
 Wednesday 11th
 March, 2020.
 Compiled:
 Wednesday 15th
 April, 2020.
 Prof. Lucchesi

R_y is known as **Rydberg energy**, whose expression reads:

$$R_y = \frac{1}{2} \frac{m e^4}{(4\pi)^2} = 12.6 \text{ eV} \quad (1.10)$$

$$R_y = \frac{1}{2} \alpha^2 m_p \quad \text{In natural units} \quad (1.11)$$

The bound states of hydrogen are arranged in levels associated with integers $n = 1, 2, 3, \dots$. Each level contains the orbital angular momentum states:

$$\begin{aligned} \ell &= 0, 1, \dots, n-1 \\ m &= -\ell, \dots, \ell \end{aligned} \quad (1.12)$$

The orbital wavefunctions are the spherical harmonics $Y_{\ell m}(\theta, \varphi)$, which are even under spatial reflection for even ℓ and odd for odd ℓ . Then, under P , these states transform as:

$$P |n\ell m\rangle = (-1)^\ell |n\ell m\rangle \quad (1.13)$$

However, with these assumptions, we are not considering that the real hydrogen atom has more structure. In fact, we are neglecting that the electron is a particle with intrinsic spin and we have to take into account also this quantity. In a more technical way, we have to add the contribution of the spin-orbit interaction (fine splitting), which is proportional to the scalar product $\vec{\mathbf{L}} \cdot \vec{\mathbf{S}}$. Concerning the Hamiltonian of this contribution, it is given by:

$$\Delta H = \frac{g-1}{2} \frac{\alpha}{m^2 r^3} \vec{\mathbf{L}} \cdot \vec{\mathbf{S}} \quad (1.14)$$

The sign is such that the state with $\vec{\mathbf{L}}$ and $\vec{\mathbf{S}}$ opposite in sign has lower energy. Moreover, it may be useful to express the operator $\vec{\mathbf{L}} \cdot \vec{\mathbf{S}}$ in terms of J^2, L^2, S^2 :

$$\vec{\mathbf{J}} = \vec{\mathbf{L}} + \vec{\mathbf{S}} \implies \vec{\mathbf{L}} \cdot \vec{\mathbf{S}} = \frac{1}{2} \left((\vec{\mathbf{L}} + \vec{\mathbf{S}})^2 - L^2 - S^2 \right) = \frac{1}{2} (J^2 - L^2 - S^2) \quad (1.15)$$

By this way it is straightforward to diagonalize the operator $\vec{\mathbf{L}} \cdot \vec{\mathbf{S}}$. At the end we get the order of magnitude of the spin-orbit interaction:

$$\left\langle \frac{\alpha}{m^2 r^3} \right\rangle \sim \frac{\alpha}{m^2 a_0^3} \sim \alpha^4 m \sim \alpha^2 R_y \quad (1.16)$$

Thus, this effect is a factor of 10^{-4} smaller than the splitting of the principal levels of hydrogen.

Another contribution that we have to add is the spin-spin interaction (hyperfine splitting) between electron and proton, which leads to the addition of another term into the total Hamiltonian. The magnetic moments of the proton and the electron interact, with the ground state favoring the configuration in which the two spins are opposite. Therefore:

$$\Delta H = C \vec{\mathbf{S}}_p \cdot \vec{\mathbf{S}}_e \quad (1.17)$$

where the C constant depends on the electron wavefunction.

Hence, we have several levels for the spin states. For example, the 1S state of hydrogen is split into two levels, corresponding to the total spin:

$$\vec{\mathbf{J}} = \vec{\mathbf{S}}_p + \vec{\mathbf{S}}_e \quad (1.18)$$

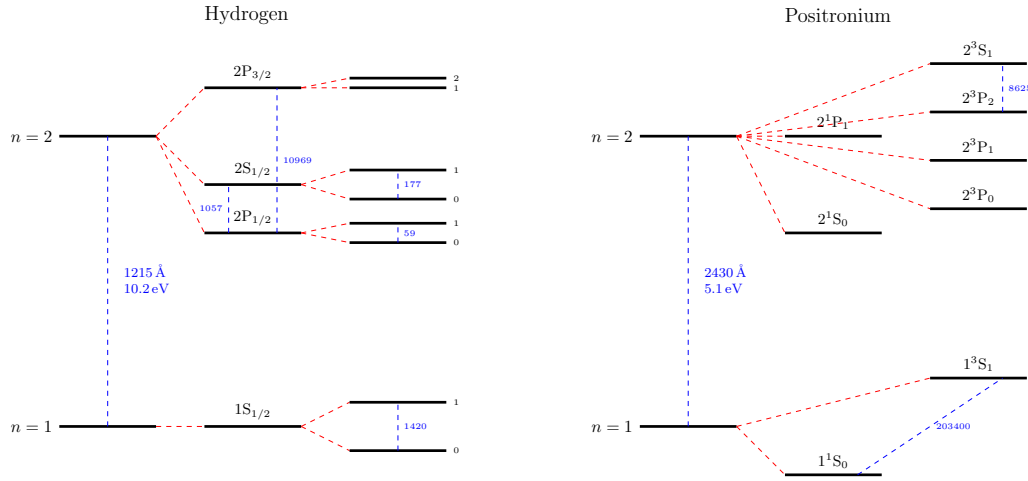


Figure 1.2: Comparison of the 1S, 2S, and 2P energy levels of hydrogen atom and positronium.

The possibilities we have are 2: $J = 0$ and $J = 1$, depending on how the two spin states of proton and electron combine. The projection on the z -axis gives 3 possibilities: $J_z = 1, 0, -1$ (corresponding to $|\uparrow\uparrow\rangle$, $\frac{1}{\sqrt{2}}(|\downarrow\uparrow\rangle + |\uparrow\downarrow\rangle)$, $|\downarrow\downarrow\rangle$).

Now the possibility that we have to evaluate is that e^+e^- forms bounded states. In fact, the same ideas can be applied to a particle-antiparticle system and the simplest case is the positronium.

It is relatively easy to make positronium. In colliders, when working with a beam of positrons which enter in the matter, they can pick up an electron and form a bounded state of positronium, so this the starting point of the idea. All the considerations applied to the case of hydrogen atom can be applied to the positronium case as well. All the calculations are omitted. The first consideration is that here we can't apply the approximation $m_p \gg m_e$, in fact the two particles here have the same mass. The solution for this two-body problem is to use the reduced mass μ , namely:

$$\mu = \frac{m_1 m_2}{m_1 + m_2} = \frac{m_e}{2} \quad (1.19)$$

At the end of all the calculations we won't do, we get that the hyperfine splitting contribution is approximately of the same of order of magnitude of the fine splitting and both are of the order $\alpha^4 m_e$.

Now we have to classify the eigenstates under parity and charge conjugation of the positronium. Let's consider first P . The intrinsic parity of the electron is $P_{e^-} = +1$, of the positron $P_{e^+} = -1$. So the parity of a single particle goes like $P = (-1)^\ell$ and the overall parity goes like $P = (-1)^{\ell+1}$.

For C , we must account three effects:

- C converts the electron to the positron and the positron to the electron. The electron and positron are fermions, and so, when we put the electron and positron back into their original order in the wavefunction, we get a factor -1 .
- Reversal of the coordinate in the orbital wavefunction gives a factor $(-1)^\ell$.
- Finally, the electron and positron spins are interchanged. The $S = 1$ state is

symmetric in spin, but the $S = 0$ state is antisymmetric.

$$\begin{aligned} S = 0 &\longrightarrow \frac{1}{2}(|\uparrow\downarrow\rangle - |\downarrow\uparrow\rangle) \\ S = 1 &\longrightarrow |\uparrow\uparrow\rangle \quad \frac{1}{2}(|\uparrow\downarrow\rangle + |\downarrow\uparrow\rangle) \quad |\downarrow\downarrow\rangle \end{aligned}$$

and so gives another factor (-1) .

In all, the positronium states have C :

$$C = (-1)^{\ell+1} \cdot \begin{cases} 1 & S = 1 \\ -1 & S = 0 \end{cases} \quad (1.20)$$

and what we get is the J^{PC} scheme. The low-lying states of the positronium spectrum then have the J^{PC} values as in Figure 1.3.

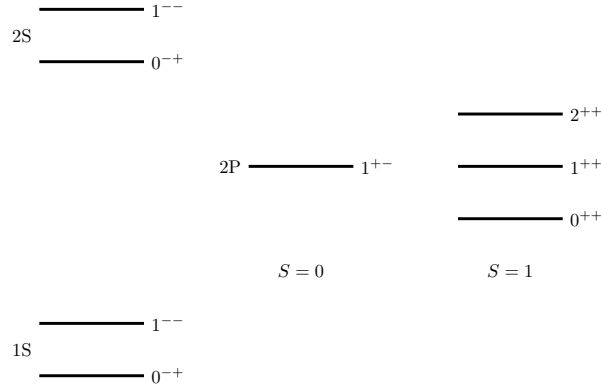


Figure 1.3: J^{PC} scheme. The 2P states 0^{++} , 1^{++} and 2^{++} arise from coupling the $L = 1$ orbital angular momentum to the $S = 1$ total spin angular momentum.

We know that electron and positron annihilate each other, so this state decays into something. The rules are E and \vec{P} conservation. It can't decay into a single photon since the momentum is not conserved. Recall that:

$$C|\gamma\rangle = -1 \implies C|n\gamma\rangle = (-1)^n \quad (1.21)$$

If we are looking for the two photon decay (so positive conjugation) of the positronium, the only possible state is the one with $S = 0$. If we are looking for a three photon decay (so negative conjugation), the only possible state is the one with $S = 1$. This kind of decay has been verified experimentally.

Positronium with state $S = 0$ is also known as **para-positronium**. If the state is $S = 1$, it is also known as **ortho-positronium**. Their medium lifes are:

$$\frac{1}{\tau_p} = \frac{1}{2}\alpha^5 m \quad \tau_p = 1.2 \cdot 10^{-10} \text{ s} \quad (1.22)$$

$$\frac{1}{\tau_o} = \frac{2}{9\pi}(\pi^2 - 9)\alpha^6 m \quad \tau_o = 1.4 \cdot 10^{-7} \text{ s} \quad (1.23)$$

So, when we emit positrons into a gas, $\frac{1}{4}$ of the states decays quickly in τ_p , while $\frac{3}{4}$ of the states decays slower in τ_o . It is a strange result, but experiment verifies it (Berko and Pendleton, 1980).

1.3 Static Quark Model

A beautifully simple way to create any particle, together with its antiparticle, is to annihilate electrons and positrons at high energy. The annihilation results in a short-lived excited state of electromagnetic fields. This state can then re-materialize into any particle-antiparticle pair that couples to electromagnetism and has a total mass less than the total energy of the annihilating e^+e^- system.

1.3.1 Light quarks: charm and beauty

By this way, the importance of the positronium state is clear. Moreover, it is linked to the discovery of quark charm and beauty.

Their discovery takes place in 1974 at SPEAR experiment, where by studying the process $e^+e^- \rightarrow hh, \mu^+\mu^-, e^+e^-$, an enormous, very narrow, resonance at about 3.1 GeV was discovered. This resonance would correspond to a new strongly interacting particle.

When they announced this discovery, they learned that the group of Samuel Ting, working at Brookhaven National Laboratory in Upton, New York, had also observed this new particle. Ting's group had studied the reaction $pp \rightarrow e^+e^- + X$, where the particles X are not observed.

This never observed particle is now called the J/ψ . A few weeks later, the SPEAR group discovered a second narrow resonance at 3686 MeV, the ψ' .

Another group of narrow resonances is found in e^+e^- annihilation at higher energy. The lightest state of this family, called Υ , has a mass of 9600 MeV. It was discovered by the group of Leon Lederman in the reaction $pp \rightarrow \mu^+\mu^- + X$ at the Fermilab proton accelerator.

Concerning the J/ψ , this particle is given by a quark doublet $c\bar{c}$ called **charmonium**. If this state exists, we will see phenomena like the ones observed with positronium. In the process $e^+e^- \rightarrow hh$, the highest rate reactions are those in which e^+e^- pair is annihilated by the electromagnetic current $\vec{j} = \bar{\psi}\vec{\gamma}\psi$ through the matrix element:

$$\langle 0 | \vec{J}(x) | e^+e^- \rangle \quad (1.24)$$

The current has spin 1, $P = -1$, and $C = -1$. These must also be properties of the annihilating e^+e^- state, and of the new state that is produced. So, all of the ψ and Υ states must have $J^{PC} = 1^{--}$.

The current creates or annihilates a particle and antiparticle at a point in space. So, if these particles are particle-antiparticle bound states, the wavefunctions in these bound states must be nonzero at the origin. Most probably, they would be the 1S, 2S, etc. bound states of a potential problem. If this guess is correct, the states with higher L must also exist. They might be produced in radiative decays of the ψ and Υ states. Indeed, there is an experimental evidence, with a pattern of states as in Figure 1.4.

Remarkably, this reproduces exactly the pattern of the lowest-energy states of positronium and makes even more clear that the analogy to positronium is precise. In the case of the ψ family, the fermion is called the charm quark (c); this quark has a mass of about 1.8 GeV. In the case of the Υ family, the fermion is called the bottom quark (b); this quark has a mass of about 5 GeV.

1.3.2 Light mesons

Now we can go back to the π mesons and other relatively light hadrons. π s are the strongly interacting particles and there are three π mesons: π^0, π^+ and π^- .

Lecture 3.
 Tuesday 17th
 March, 2020.
 Compiled:
 Wednesday 15th
 April, 2020.
 Prof. Lucchesi

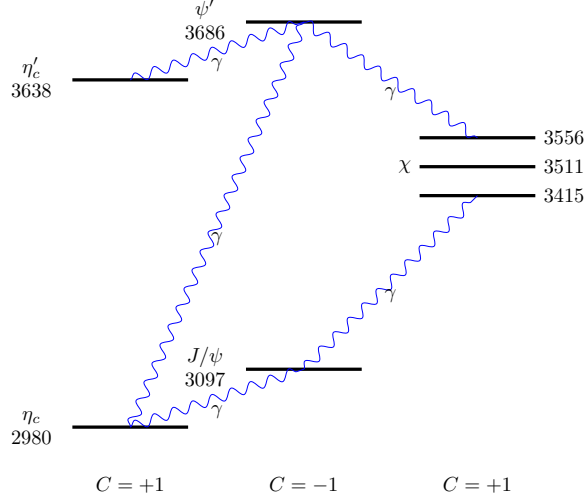
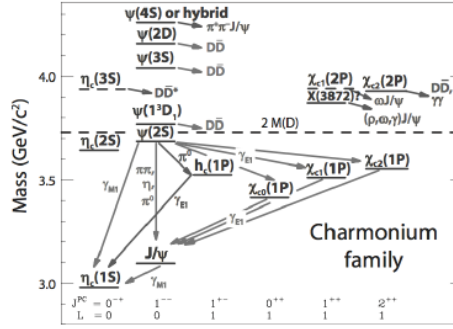
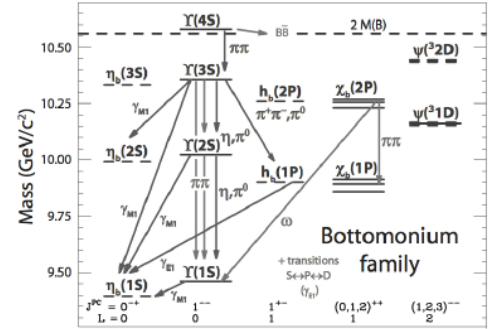


Figure 1.4: Pattern of states for the charmonium.

Figure 1.5: Observed states and transitions of the J/ψ system.Figure 1.6: Observed states and transitions of the Υ system.

Their history is the beginning of modern particle physics and they were discovered in 1947, when Lattes, Occhialini and Powell demonstrated the existence of π^\pm through $\pi^\pm \rightarrow \mu^\pm + \nu$.

By detailed study of their interactions, it was determined that the π mesons also had $J^P = 0^-$. The π^0 decays to 2 photons, so it is $C = +1$. All of this is consistent with the interpretation of the pions as spin- $\frac{1}{2}$ fermion-antifermion bound states.

There are 9 relatively light 0^- hadrons, also known as **pseudoscalar mesons**, and 9 somewhat heavier 1^- hadrons, called the **vector mesons**, presented in Figure 1.7. The K and K^* states are not produced singly in strong interactions. They are only produced together with one another, or with special excited states of the proton. For example, we see the reactions:

$$\begin{aligned}\pi^- p &\rightarrow n K^+ K^- \\ \pi^- p &\rightarrow \Lambda^0 K^0\end{aligned}$$

where Λ^0 is a heavy excited state of the proton, but we don't see the reaction:

$$\pi^- p \rightarrow n K^0$$

For this reason, the K mesons and the Λ^0 baryon became known as the strange particles.

As a consequence of this discovery, a new quantum number, the **strangeness**, was introduced to describe the production and decay processes. It was found that the

<u>η'</u>				958					
<u>η</u>				548	<u>ϕ^0</u>				1020
<u>K^-</u>	<u>\bar{K}^-</u>	<u>K^0</u>	<u>K^+</u>	498	<u>K^{*-}</u>	<u>\bar{K}^{*0}</u>	<u>K^{*0}</u>	<u>K^{*+}</u>	892
					<u>ω^0</u>				781
<u>π^-</u>	<u>π^0</u>	<u>π^+</u>		140	<u>ρ^-</u>	<u>ρ^0</u>	<u>ρ^+</u>		770

Figure 1.7: Light mesons summary. On the left there are the pseudoscalar mesons, on the right the vector mesons. The numbers given are the masses of the particles in MeV.

rules for K and K^* production can be expressed simply by saying that the strong interaction preserves the strangeness, with K^0 , K^+ , K^{*0} and K^{*+} having strangeness $S = -1$, their antiparticles having $S = +1$, and the Λ^0 having $S = +1$. Moreover, with the introduction of strangeness, a new kind of quark was introduced in the theories, namely the strange quark s . States with strangeness $+1$ will be assigned one s quark, and states with strangeness -1 will have one \bar{s} antiquark.

1.4 Leptons

The leptons are fundamental particles, divided in several classes. We have:

- **Electron e .**

It was discovered by J.J. Thomson in 1897 while studying the properties of cathode rays.

- **Muon μ .**

It was discovered by Carl D. Anderson and Seth Neddermeyer in 1936 as component of the cosmic rays. At the beginning it was thought to be the Yukawa particle, the mediator of the strong force. Then Conversi, Pancini and Piccioni gave a proof that it does not interact strongly.

- **Tauon τ .**

It was discovered by a group led by Martin Perl at Stanford Linear Accelerator Center. They used e^+e^- collisions with final states events $e\mu$.

- **Neutrino ν .**

Neutrino hypothesis was formulated by Pauli to explain the β -decay. It was discovered by Clyde Cowan and Fred Reines in the 1953. We don't know if mass is given to neutrinos through the same mechanism (Higgs mechanism) for the other particles or if there is something that does it that we still don't know.

Chapter 2

Tools for calculations

To compare the results of elementary particle experiments to proposed theories of the fundamental forces, we must think carefully about what quantities we can compute and measure. We cannot directly measure the force that one elementary particle exerts on another. Most of our information about the subnuclear forces is obtained from scattering experiments or from observations of particle decay.

In scattering experiments, the basic measureable quantity is called the **differential cross section**. In particle decay, the basic measureable quantity is called the **partial width**.

2.1 Observables in experimental particle physics

The basic observable quantity associated with a decaying particle is the **rate of decay**. In quantum mechanics, an unstable particle A decays with the same probability in each unit of time. The probability of survival to time t then obeys the differential equation:

$$\frac{dP(t)}{dt} = -\frac{P}{\tau_A} \xrightarrow{\text{solution}} P(t) = P_0 e^{-\frac{t}{\tau_A}} \quad (2.1)$$

The decay rate τ_A^{-1} is also called the **total width** Γ_A of the state A . Its dimension is 1/sec, equivalent to GeV up to factors of \hbar and c .

$$\tau_A = \frac{1}{\Gamma_A} \quad \Gamma_A = \text{Total width of the state } A \quad (2.2)$$

If there are multiple decay processes like $A \rightarrow f$, each process has a rate $\Gamma(A \rightarrow f)$, namely the **partial width**. Thus, the total decay rate is given by:

$$\Gamma_A = \sum_f \Gamma(A \rightarrow f) \quad (2.3)$$

Another quantity called **branching ratio** can be defined by the definition of the previous ones:

$$\frac{\Gamma(A \rightarrow f)}{\Gamma_A} = \text{Branching ratio} \quad (2.4)$$

We can now introduce the **cross section**. Let's imagine a fixed target experiment, where a beam of A particles of density n_A and velocity v_A , are shot at the fixed center B . What we can measure includes the rate R at which we see scatterings from the beam:

$$R = \frac{\text{Number of events}}{\text{Time}} = n_A v_A \sigma_i \quad (2.5)$$

with σ_i the cross section of the process, which has the dimension of an area and it is measured in barn (10^{-28} m^2). It is the effective area that the target B presents to the beam. Another important quantity is the **luminosity**, i.e.:

$$\mathcal{L} = \frac{R}{\sigma_i} \quad (2.6)$$

Returning to the cross section, an alternative definition can be given. Imagine two bunches of particles A and B aimed at one another, namely a collision between two beams. The key idea is that the second beam is the target, so we consider $N_B = n_B l_B A_B$ in order to calculate the rate:

$$R = n_A n_B l_B A_B |v_A - v_B| \sigma_i \quad (2.7)$$

As pointed before, every beam is composed of bunches with the following gaussian distributuion:

$$\frac{dN}{ds} = \frac{N}{2\pi\sigma_x\sigma_y} e^{-\left(\frac{x^2}{2\sigma_x^2} + \frac{y^2}{2\sigma_y^2}\right)} \quad (2.8)$$

The number of interations per bunch is $N_{\text{int}} = \sigma_{\text{int}} \frac{N_1 N_2}{4\pi\sigma_x\sigma_y}$ and the bunch frequency is f . Therefore, we can calculate the rate:

$$R_i = N_{\text{int}} f = \sigma_{\text{int}} \frac{N_1 N_2}{4\pi\sigma_x\sigma_y} \quad (2.9)$$

2.2 Partial Width and Cross Section calculation

The partial width and the cross section for a certain process can be calculated through **Fermi's Golden Rule** in a very practical way. By using the time evolution operator T , we can write:

$$\langle 1, 2, \dots, n | T | A(p_A) \rangle = \underbrace{\mathcal{M}(A \longrightarrow 1, 2, \dots, n)}_{\text{Invariant matrix element}} \underbrace{(2\pi)^4 \delta^{(4)}\left(p_A - \sum_{i=1}^n p_i\right)}_{E, \vec{p} \text{ conservation}} \quad (2.10)$$

It is useful to work out the dimension of \mathcal{M} . The operator T is dimensionless, and the states have total dimension $\text{GeV}^{-(n+1)}$. The delta function has units GeV^{-4} . Then the invariant matrix element has the units:

$$\mathcal{M} \sim \text{GeV}^{3-n} \quad (2.11)$$

Now, to find the total rate, we must integrate over all possible values of the final momenta. This integral is called **phase space** and for n final particles, the expression for the phase space integral is:

$$\int d\Pi_n = \int \frac{d^3 p_1}{(2\pi)^3 2E_1} \cdots \frac{d^3 p_n}{(2\pi)^3 2E_n} (2\pi)^4 \delta^{(4)}\left(p_A - \sum_{i=1}^n p_i\right) \quad (2.12)$$

However, we also need to normalize. So the initial state $|A\rangle$ will yield:

$$|A\rangle \longrightarrow \frac{1}{2E_A} \quad \text{Initial state} \quad (2.13)$$

Finally, the Fermi Golden Rule formula for a partial width to an n -particle final state f is:

$$\Gamma(A \longrightarrow f) = \frac{1}{2M_A} \int d\Pi_n |\mathcal{M}(A \longrightarrow f)|^2 \quad (2.14)$$

If the final state particles have spin, we need to sum over final spin states. The initial state A is in some state of definite spin. If we have not defined the spin of A carefully, an alternative is to average over all possible spin states of A . By rotational invariance, the decay rate of A can't depend on its spin orientation.

Concerning the cross section, a formula for this quantity is constructed in a similar way. We need the matrix element for a transition from the two initial particles A and B to the final particles through the interaction. So, it reads:

$$\sigma(A + B \longrightarrow f) = \frac{1}{2E_A E_B |v_A - v_B|} \int d\Pi_n |\mathcal{M}(A + B \longrightarrow f)|^2 \quad (2.15)$$

2.3 Phase Space integral calculation

Phase space plays a very important role in particle physics. The default assumption is that final state particles are distributed according to phase space. This assumption is correct unless the transition matrix element has nontrivial structure. We will proceed with a couple of examples/exercises in order to understand the way of working with this kind of computations.

Example 1: Phase space of 2 particles

Most of the reactions we will discuss will have two particles in the final state. So it's better to start with this example. We have to compute:

$$\int d\Pi_2 = \int \frac{d^3 p_1}{(2\pi)^3 2E_1} \frac{d^3 p_2}{(2\pi)^3 2E_2} (2\pi)^4 \delta^{(4)}(p - p_1 - p_2) \quad (2.16)$$

Let's work in the CM system, where $\vec{p}_1 + \vec{p}_2 = 0$ and so $\vec{p}_1 = -\vec{p}_2$. Hence:

$$P = (E_{\text{CM}}, \vec{0}) \quad (2.17a)$$

$$p_1 = (E_1, \vec{p}) \quad (2.17b)$$

$$p_2 = (E_2, -\vec{p}) \quad (2.17c)$$

We have to integrate over \vec{p}_2 and exploit the properties of δ function:

$$\begin{aligned} \int d\Pi_2 &= \int \frac{d^3 p}{(2\pi)^3} \frac{1}{2E_1 2E_2} (2\pi) \delta(E_{\text{CM}} - E_1 - E_2) \\ &= \int \frac{p^2 d\Omega}{16\pi^2 E_1 E_2} \frac{E_1 E_2}{p E_{\text{CM}}} \\ &= \frac{1}{8\pi} \left(\frac{2p}{E_{\text{CM}}} \right) \int \frac{d\Omega}{4\pi} \end{aligned} \quad (2.18)$$

Example 2: Phase space of 3 particles

It is also possible to reduce the expression for three-body space to a relatively simple formula. Let's work again in the center of mass frame where $\vec{p}_1 + \vec{p}_2 + \vec{p}_3 = 0$ and let the total energy-momentum in this frame be $Q^0 = E_{\text{CM}}$. The three momentum vectors lie in the same plane, called **event plane**. Then the phase space integral can be written as an integral over the orientation of this plane and over the variables:

$$x_1 = \frac{2E_1}{E_{\text{CM}}} \quad x_2 = \frac{2E_2}{E_{\text{CM}}} \quad x_3 = \frac{2E_3}{E_{\text{CM}}}$$

which obey the constraint:

$$x_1 + x_2 + x_3 = 2$$

It can be shown that, after integrating over the orientation of the event plane, the integral over three-body phase space can be written as:

$$\int d\Pi_3 = \frac{E_{\text{CM}}^2}{128\pi^3} \int dx_1 dx_2 \quad (2.19)$$

It can be shown, further, that this integral can alternatively be written in terms of the invariant masses of pairs of the three vectors ($m_{12}^2 = (p_1 + p_2)^2$ and $m_{23}^2 = (p_2 + p_3)^2$):

$$\int d\Pi_3 = \frac{1}{128\pi^3 E_{\text{CM}}^2} \int dm_{12}^2 dm_{23}^2 \quad (2.20)$$

This formula leads to an important construction in hadron physics called the **Dalitz plot**.

Example 3: $\pi^+\pi^- \longrightarrow \rho^0 \longrightarrow \pi^+\pi^-$

One important type of structure that one finds in scattering amplitudes is a **resonance**. In ordinary quantum mechanics, a resonance is described by the **Breit-Wigner formula**:

$$\mathcal{M} \sim \frac{1}{E - E_{\text{R}} + \frac{i}{2}\Gamma} \quad (2.21)$$

where E_{R} is the energy of the resonant state and Γ is its decay rate. The Fourier transform of Eq. 2.21 is:

$$\psi(t) = ie^{-iE_{\text{R}}t} e^{-\Gamma \frac{t}{2}} \quad (2.22)$$

Then the probability of maintaining the resonance decays exponentially

$$|\psi(t)|^2 = e^{-\Gamma t} \quad (2.23)$$

corresponding to the lifetime:

$$\tau_{\text{R}} = \frac{1}{\Gamma} \quad (2.24)$$

It is useful to consider a specific example of a resonance in an elementary particle reaction, so we will consider $\pi^+\pi^- \longrightarrow \rho^0 \longrightarrow \pi^+\pi^-$, where the meson ρ^0 is found as a resonance at the ρ^0 mass of 770 MeV. We can represent this process by a diagram of evolution in space-time, as in Figure 2.1.

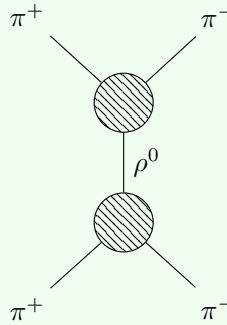


Figure 2.1: Diagram of $\pi^+\pi^- \longrightarrow \rho^0 \longrightarrow \pi^+\pi^-$.

Briefly, what we find is that the final distributions of the invariant masses are not in agreement with what we expect from the phase space distributions for two particles. In this case we can do the calculation in an easy way by studying:

1. $\pi^+\pi^- \longrightarrow \rho^0$ and treat it as a stable particle
2. Using Feynman diagrams.

So, if we consider the cross section of $\pi^+\pi^- \longrightarrow \rho^0$, we get:

$$\sigma(\pi^+\pi^- \rightarrow \rho^0) = \frac{1}{4E_A E_B |v_A - v_B|} \int \frac{d^3 p_C}{(2\pi)^3 2E_C} |\mathcal{M}|^2 (2\pi)^4 \delta^4(p_C - p_A - p_B) \quad (2.25)$$

where $A = \pi^+$, $B = \pi^-$ and $C = \rho^0$. The partial width reads:

$$\Gamma_\rho = \frac{1}{2m_\rho} \int d\Pi_2 |\mathcal{M}|^2 = \frac{g_\rho^2}{6\pi} \frac{p^3}{m_\rho^2} \quad (2.26)$$

By studying the cross section of the whole process $\pi^+\pi^- \longrightarrow \rho^0 \longrightarrow \pi^+\pi^-$, we get:

$$\sigma(\pi^+\pi^- \longrightarrow \rho^0 \longrightarrow \pi^+\pi^-) = \frac{1}{2m_\rho} \frac{1}{8\pi} \frac{2p}{m_\rho} \int \frac{d\Omega}{4\pi} \frac{1}{(E_{\text{CM}}^2 - m_\rho^2)^2 - m_\rho^2 \Gamma_\rho^2} |k|^2 \quad (2.27)$$

where k is a part related to the spin of ρ^0 .

We see a resonance and we are able to fit the data, so we can get the quantities we want to know as the parameters of the best fit.

Chapter 3

Detectors for Particle Physics

3.1 Recap: interaction of particles with matter

The way we identify particles is through their interaction with matter. So, we can detect:

- Charged particles based on ionization, bremsstrahlung, Cherenkov effect.
- γ -rays based on photoelectric/Compton effect and pair production.
- Neutrons based on strong interaction.
- Neutrinos based on weak interaction.

We will give only a phenomenological treatment since the goal is to be able to understand the implications for detector design.

3.1.1 Interactions involving the electrons and heavier particles

A relativistic charged particle with a mass much greater than the mass of the electron, when passing through the matter, is subject to a loss of energy due to the interaction with atomic electrons. These ones can be subtracted from the atom and then can be detected. From the total charge collected by the electrodes of a detector, it is possible to know the original interacting particle. The equation that describes this interaction and the loss of energy is the **Bethe-Bloch Equation** (in natural units):

$$-\left\langle \frac{dE}{dx} \right\rangle = K \rho \frac{Z}{A} \frac{z^2}{\beta^2} \left[\frac{1}{2} \log \frac{2m_e c^2 \beta^2 \gamma^2 T_{\max}}{I^2} - \beta^2 - \frac{\delta(\beta\gamma)}{2} - \frac{C}{z} \right] \quad (3.1)$$

where the meaning of the various symbols is given in Table 3.1. A plot showing the stopping power in function of the factor $\beta\gamma$ is given in Figure 3.1. In particular, from this plot we can see some interesting characteristics of the energy loss process. In the first part, the particle loses more energy when its velocity is slower, so the trend is $\sim \frac{1}{\beta^2}$. When the energy increases, a minimum is met, whose x -axis value is approximately the same for every material. The right part of the plot with respect to this minimum shows a gain in the energy loss which is due to relativistic effects.

The Bethe-Bloch formula is valid for particles much heavier than the electron. For this kind of particles, we have that relativistic effects even at low energies, since its mass is lower in comparison with the other particles. So, the electron loses energy through ionization (at lower energies) and **bremsstrahlung**, namely *braking radiation*, when deflected by another charged particle (at higher energies). The different materials that the electron can pass through, are characterized by their **radiation length** X_0 ,

Lecture 4.

Wednesday 18th
March, 2020.

Compiled:

Wednesday 15th
April, 2020.

*Interaction
through ionization*

*Bremsstrahlung
energy loss*

Symbol	Physical meaning
K	Constant [$0.307075 \text{ MeV g}^{-1} \text{ cm}^2$]
ρ	Density of the absorber
Z	Atomic number of absorber
A	Atomic mass of absorber
z	Atomic number of incident particle
β	Particle velocity in units of c
γ	Relativistic factor derived from β
T_{\max}	Maximum energy transfer in a single collision
I	Ionization potential of the absorber

Table 3.1: Bethe-Bloch formula: meaning of all the symbols figuring in its expression.

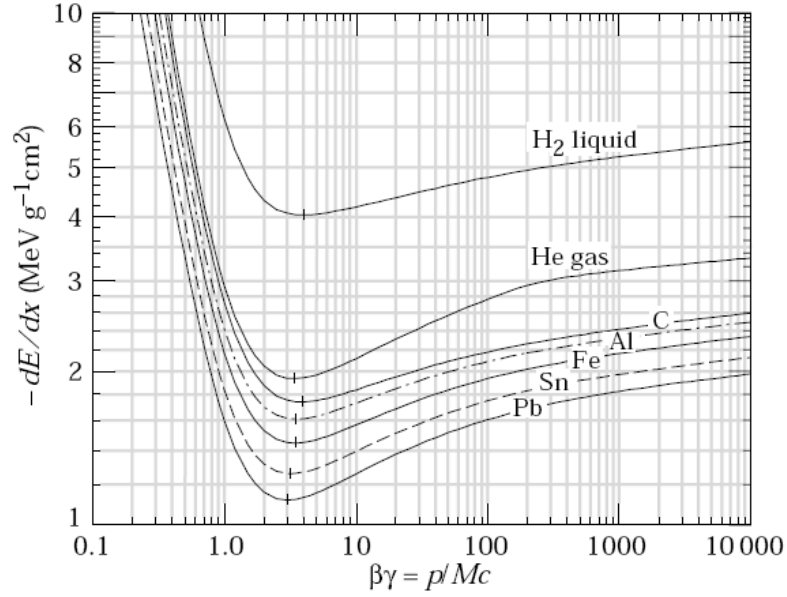


Figure 3.1: Few examples for different materials of Bethe-Bloch formula.

which is a quantity empirically defined as the distance covered by an electron beam before its energy decreases by a factor $\frac{1}{e}$ (63%). It is measured in g/cm^2 and an approximation of its expression is:

$$X_0 = \frac{A}{4\alpha N_A Z^2 r_e^2 \log \frac{183}{Z^{\frac{1}{3}}}} \quad (3.2)$$

Moreover, there exists a point in which the loss of energy due to ionization and the loss of energy due to bremsstrahlung are equal. This point is called **critical energy** E_c and a relatively good approximation of its value is:

$$E_c \approx \frac{600 \text{ MeV}}{Z} \quad (3.3)$$

Energy loss as a
function of other
parameters

Concerning the trend of these losses, we find that the ionization loss decreases logarithmically with E and increases linearly with Z , while bremsstrahlung loss increases approximately linearly with E and it is the dominant process at high energies. This is evident in the plots in Figures 3.2 and 3.3.

3.1.2 Interaction of photon with the matter

Photons can lose energy in several ways. The possibilities are:

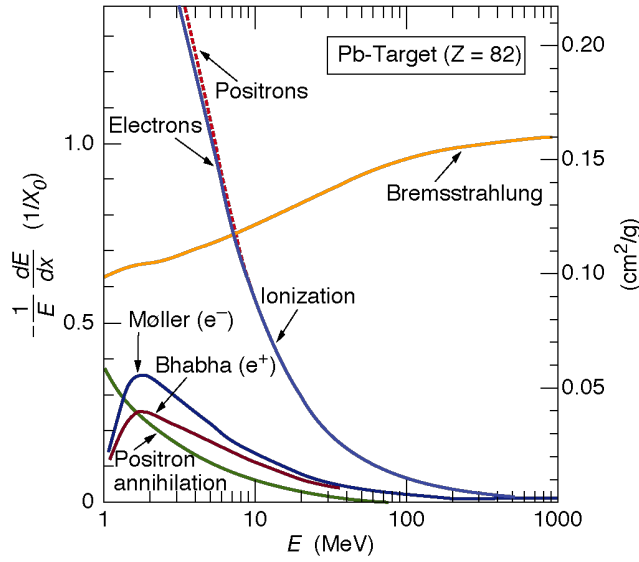


Figure 3.2: Total energy loss for electrons.

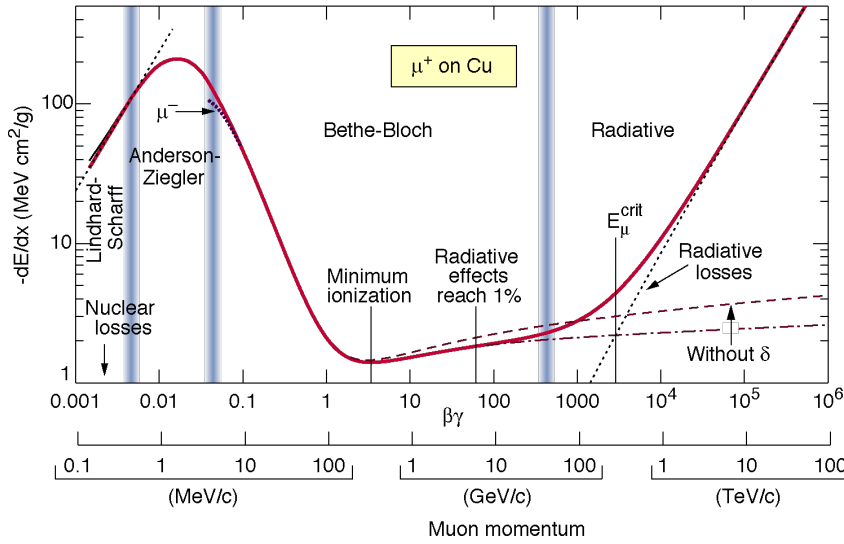


Figure 3.3: Energy loss summary.

- Photoelectric effect on atoms at low energy.
- Compton effect, which is important at medium range energies.
- Pair production, which is the dominant process at higher energies.

It goes without saying that we will focus on pair production, since we are discussing topics whose energies are relatively high. Concerning the cross section of this process, it is approximated by:

$$\sigma_{\text{pair}} = \frac{7}{9} \frac{N_A}{A} \frac{1}{X_0} \quad (3.4)$$

We can characterize a certain material by defining the **attenuation length** λ , namely the length for which the beam of photons inside the material is attenuated by a factor $\frac{1}{e}$, and it is linked to the radiation length by $\lambda = \frac{9}{7} X_0$.

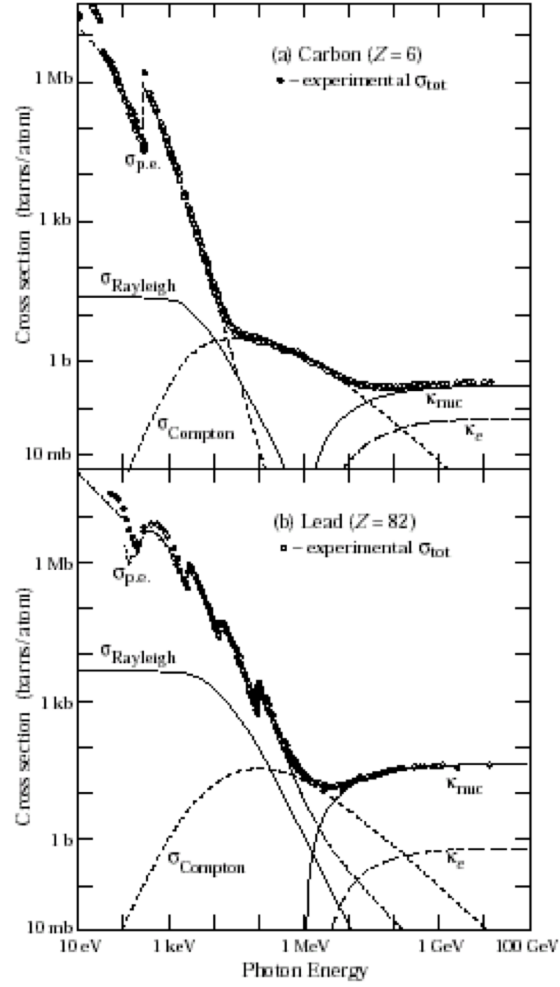


Figure 3.4: Interaction of photons with matter.

3.2 Gaseous, scintillator and solid state detectors

Particles can be identified as point-like objects with a certain mass and some other properties that characterize them. The only way to detect them is to make them interact inside a medium. With this technique we can measure their charge, medium lifetime, velocity, momentum and energy and from these we can retrieve their mass and a lot of other interesting properties. So, let's start a discussion on the many types of detectors that can be employed for a particle experiment.

3.2.1 Gas detectors

These detectors are based on the interaction of the particles with a gaseous medium. The interaction causes the ionization of the atoms in the medium, the charge is collected and from its total amount we can reconstruct the properties of the interacting particles.

In particular, we focus now on the ionization process. When the particle enters in the medium, a first ionization takes place and it is called **primary ionization**. For example, it can be schematized as follows:



The charges produced in the primary ionization interacts as well with the medium

and they create a **secondary ionization**, as follows:

$$X + e^- \longrightarrow X^+ + e^- + e^- \quad (3.6)$$

Experimentally speaking, it is important to evaluate the number of particles produced in the interaction and the relevant parameters to estimate this quantity are the ionization energy E_i , the average energy/ion pair W_i and the average number of ion pairs (per cm) n_T . By putting all together, we get:

$$\langle n_T \rangle = \frac{L \langle \frac{dE}{dx} \rangle}{W_i} \quad (3.7)$$

with L the thickness of the material. Typical values for E_i and n_T are:

$$E_i \sim 30 \text{ eV}$$

$$n_T \sim 100 \frac{\text{pairs}}{3 \text{ KeV}}$$

Another important effect to discuss in gas detectors is the **diffusion** in presence of electric and/or magnetic fields. These fields affect the trajectory of the particles transversally and longitudinally. In particular, by measuring the bending of the particle in presence of a magnetic field with a component orthogonal to the velocity vector, we are able to infer the momentum of the particle itself. The electric field influences only the longitudinal diffusion and not the transverse diffusion.

Lastly, another phenomenon that can happen in gas detectors is the **multiplication**. The electrons can undergo to a multiplication process called **Townsend avalanche**. Given the number of electrons at the position x , $n(x) = n_0 e^{\alpha x}$, we have the gain:

$$G = \frac{n(x)}{n_0} = e^{\alpha x} \quad (3.8)$$

where the parameter α can depend on x .

Depending on the gain factor G of the multiplication, four regions of work of the detector can be exploited:

- **Ionization mode**

The intensity of the electrical field E is low and the electric current at the electrodes of the detector is proportional to the charge produced in primary ionization.

- **Proportional mode**

It's the region of use for most of detectors and in this case E is sufficiently intense to generate a secondary ionization, so that the initial charge can be multiplied by a certain factor. It's also possible to measure the loss of energy of the original particle, proportional to the collected charge.

- **Limited proportional mode**

The amplification of ionization charge is now a process that can't be controlled since the electric field is too strong.

- **Geiger mode**

The electric field is so intense to generate an avalanche of electrons without control, that reaches the electrodes. It is not possible to measure the energy loss in this case, but we can only detect a logic signal that tells us if a particle has crossed the detector or not.

Ionization mode:

full charge collection
no multiplication; gain ≈ 1

Proportional mode:

multiplication of ionization
signal proportional to ionization
measurement of dE/dx
secondary avalanches need quenching;
gain $\approx 10^4 - 10^5$

Limited proportional mode:

[saturated, streamer]

strong photoemission
requires strong quenchers or pulsed HV;
gain $\approx 10^{10}$

Geiger mode:

massive photoemission;
full length of the anode wire affected;
discharge stopped by HV cut

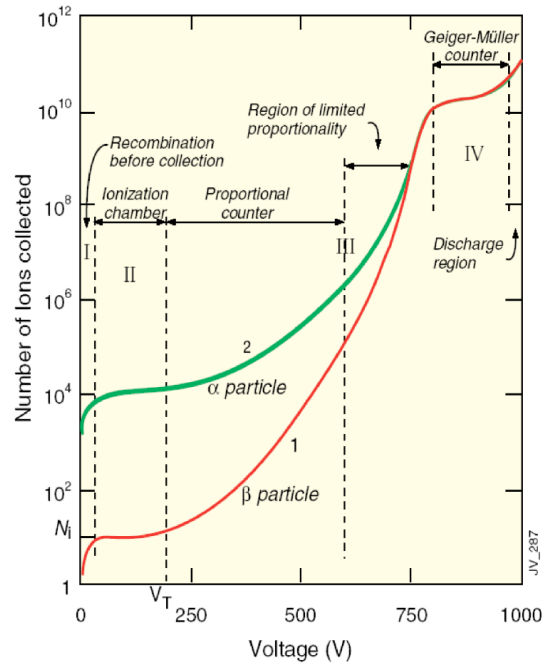


Figure 3.5: Regions of work of ionization detector with a plot giving numeric and practical examples.

3.2.2 Multiwire proportional chambers

They are proportional chambers with multiple wires added to reconstruct the trajectory of the particle. The cathode is the external shell, while the anodes are the internal wires, which generate an electrical field in first order approximation inversely proportional to the distance from the wire.

Schematic setup:

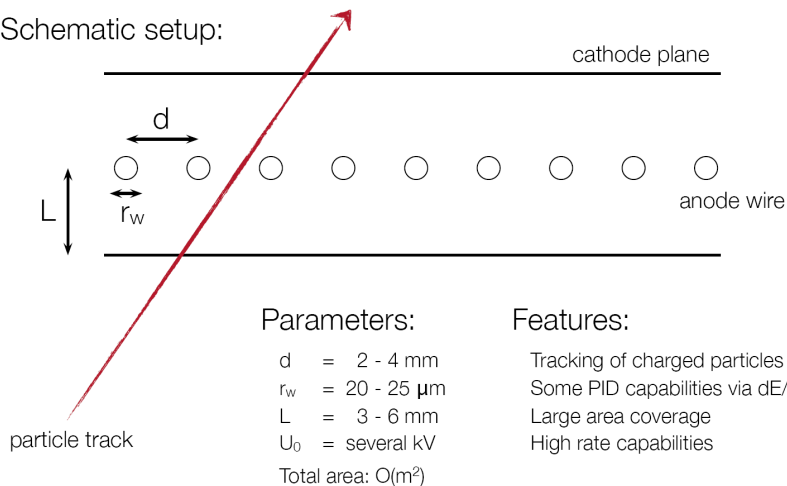


Figure 3.6: Description of multiwire proportional chamber structure and principle of work.

The principle of work is quite simple. The passage of a certain particle produces ionization charges, in particular electrons, which are collected by the nearest wire. Knowing which are all the anodes that collected ionization charge, we can understand the path followed by the crossing particle.

3.2.3 Drift chambers

Drift chambers are very similar to multiwire proportional chambers, however in this case we can have two dimensional informations through time measurements, namely **drift time** measurements.

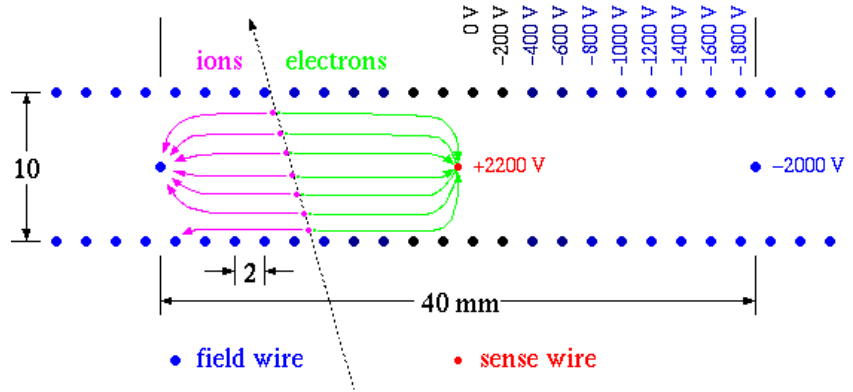


Figure 3.7: Scheme of a drift chamber.

They exploit an external detector such as a scintillator counter, near the chamber, to determine the time t_0 in which the particle arrives. The scintillator detects it and sends a signal to start a sort of chronometer. Then the particle cross the chamber and the electrons from the ionization drift to the nearest anode, captured by the electrical field. At the arrival of the electrons at the anode, a singals is sent to stop the time measurement. Now we have all the informations to extrapolate the drift time t_D , from which we can compute the spatial informations:

$$x = \int_0^{t_D} v_D dt \quad (3.9)$$

What is important to remember is that the detector is built with a studied geometry in order to get a known drift velocity.

3.2.4 Semiconductor detectors

Semiconductor detectors have the following characteristics:

- High density (respect to gas detectors), so large energy loss in a shorter distance.
- A small diffusion effect, so their position resolution can be less than 10 μm .
- Low ionization energy, so it is easier to produce charged particles when they are crossed.

The materials employed for their construction can vary depending on the purpose of the detector itself. The possibilities are:

- Germanium, which needs to be operated at a very low temperature (77 K) due to small band gap in its microscopic structure.
- Silicon, which can operate at room temperature.
- Diamond, resistant to very hard radiations, with low noise signal. Its employment is still limited by a high cost of natural diamonds, however there exist some techniques through which the artificial production of diamond is a reality. So, diamond detectors are in development up to now.

Silicon detectors are the most common and they are based on a p-n junction with reverse bias applied to enlarge the depletion region. The potential barrier becomes higher so that the diffusion current across the junction is suppressed and the current across the junction is very small (“leakage current”).

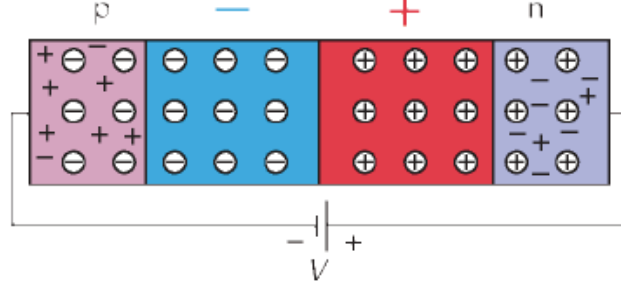


Figure 3.8: A p-n junction with reverse bias applied.

Such a detector can be built in strips. By segmenting the implant we can reconstruct the position of the traversing particle in one dimension. We have a higher field close to the collecting electrodes where most of the signal is induced. Strips can be read with dedicated electronics to minimize the noise.

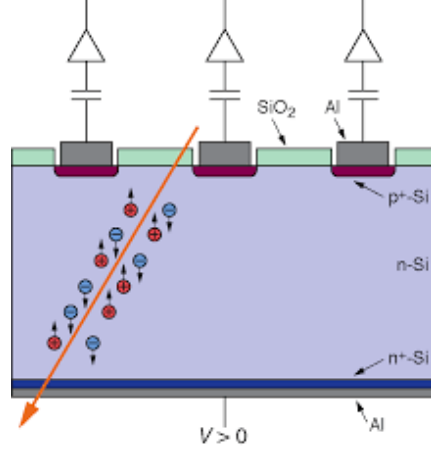


Figure 3.9: Silicon microstrip detector section with representation of ionization charges, generated by a traversing particle.

To have 2-dimensional measurements, double sided silicon detector are used. Moreover, a type of silicon detector still in development is the pixel detector (for 3-dimensional measurements).

Noise contributions can be leakage current and electronics readout. Instead, position resolution is the spread of the reconstructed position minus the true position. For example:

$$\sigma = \frac{\text{pitch length}}{\sqrt{12}} \quad \text{One strip cluster} \quad (3.10)$$

$$\sigma = \frac{\text{pitch length}}{1.5 \frac{S}{N}} \quad \text{Two strip cluster} \quad (3.11)$$

3.3 Track reconstruction

Track reconstruction is used to determine momentum of charged particles by measuring the bending of a particle trajectory in a magnetic field. The starting point is the

expression of the Lorentz force to which a particle is subjected when moving inside a magnetic field:

$$\vec{F} = q\vec{v} \times \vec{B} \quad (3.12)$$

from which we get:

$$m \frac{v^2}{r} = qvB \implies p = rqB \quad (3.13)$$

In fixed target experiments, Eq. 3.13 can be rewritten to:

$$p = qB \frac{L}{\theta} \quad (3.14)$$

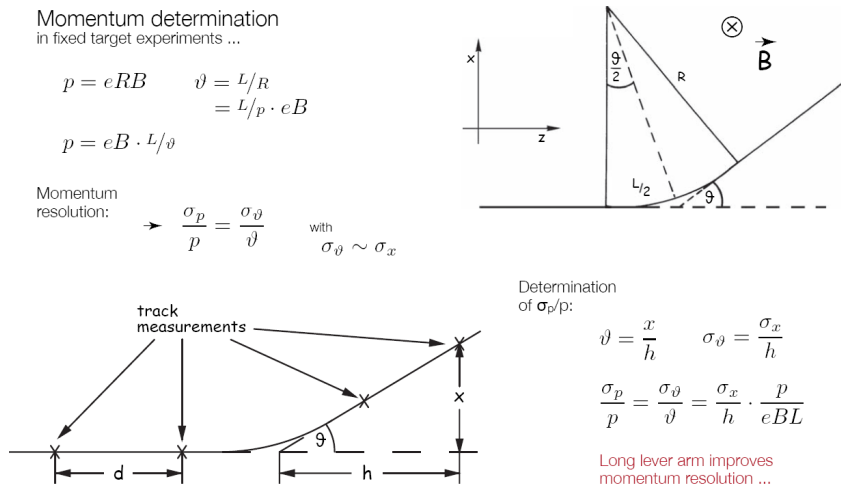


Figure 3.10: Tracking reconstruction example.

3.4 Calorimetry

Conceptually, a calorimeter is a block of matter, which intercepts the primary particle and is of sufficient thickness to cause it to interact and deposit all its energy inside the detector volume in a subsequent cascade or "shower" of increasingly lower-energy particles. Eventually most of the incident energy is dissipated and appears in the form of heat. Some (usually a very small) fraction of the deposited energy goes into the production of a more practical signal (e.g. scintillation light, Cerenkov light, or ionization charge), which is proportional to the initial energy.

In principle, the uncertainty in the energy measurement is governed by statistical fluctuations in the shower development, and the fractional resolution $\frac{\sigma}{E}$ improves with increasing energy E as $E^{-\frac{1}{2}}$.

At the outset it was noted that calorimetric detectors offer many other attractive capabilities, aside from the energy response, all of which have since been exploited in varying degrees:

- They are sensitive to charged and neutral particles
- The size of the detector scales logarithmically with the particle energy E , whereas for magnetic spectrometers the size scale with momentum p as $p^{\frac{1}{2}}$, for a given relative momentum resolution $\frac{\Delta p}{p}$.

Lecture 5.
Tuesday 24th
March, 2020.
Compiled:
Wednesday 15th
April, 2020.

Main features of
calorimeters

- Through the use of segmented detectors the information of the shower development allows precise measurements of the position and angle of the incident particle.
- The shower development is a statistical process and the number of secondary particles $\langle N \rangle$ is proportional to the energy E of the incident particle.
- The different response of the materials to electrons, muons and hadrons can be exploited for particle identification.
- Their fast time response allows operation at high particle rates, and the patterns of energy deposition can be used for real-time event selection.

3.4.1 Electromagnetic shower development

The theory of electromagnetic shower development is relatively simple. Electrons and positrons lose energy by ionization and by radiation. The first process dominates at low energy, the second one at high energy. Photons interact either through the photoelectric effect, Compton scattering or pair production. The photoelectric effect dominates at low energies, pair production at high energies. So in our case, for electrons the loss of energy is dominated by bremsstrahlung, for photons by pair production.

E.M. shower model

A simplified electromagnetic shower model in a homogeneous detector has the following assumptions: we assume a material with radiation length of X_0 and we suppose that we have 2^t particles after $t \cdot X_0$ radiation lengths, each with energy $\frac{E}{2^t}$. So the shower stops when $E < E_C$ and the number of particles generated along the path is:

$$N_{\max} = 2^{t_{\max}} = \frac{E_0}{E_C} \quad (3.15)$$

The maximum expansion of the shower is obtained at:

$$t_{\max} \propto \log \left(\frac{E_0}{E_C} \right) \quad (3.16)$$

Molière radius

The lateral development of the shower is described by the **Molière Radius** ρ_M :

$$R_M \approx (21 \text{ MeV}) \frac{X_0}{E_C} \quad (3.17)$$

It is important to note that both X_0 and ρ_M are defined for the asymptotic energy regime ($> 1 \text{ GeV}$).

Transversally, the 95% of the energy of shower is contained in a cone of radius $R \sim 2\rho_M$. For lateral shower containment, material differences are much smaller than longitudinally. In addition, there is no energy dependence. A given (sufficiently long) cylinder will thus contain the same fraction of the energy from 1 GeV electromagnetic showers as from 1 TeV ones. Some examples are showed in Figures 3.11 and 3.12.

3.4.2 Hadronic shower development

Nuclear interaction length

Showers generated and developed by hadrons are affected by strong interactions, characterized by the **nuclear interaction length** λ_{int} , namely the average distance hadrons travel before inducing a nuclear interaction. It is expressed in g/cm² and for energies up to 100 GeV it scales as:

$$\lambda_{\text{int}} \sim A^{\frac{1}{3}} \quad (3.18)$$

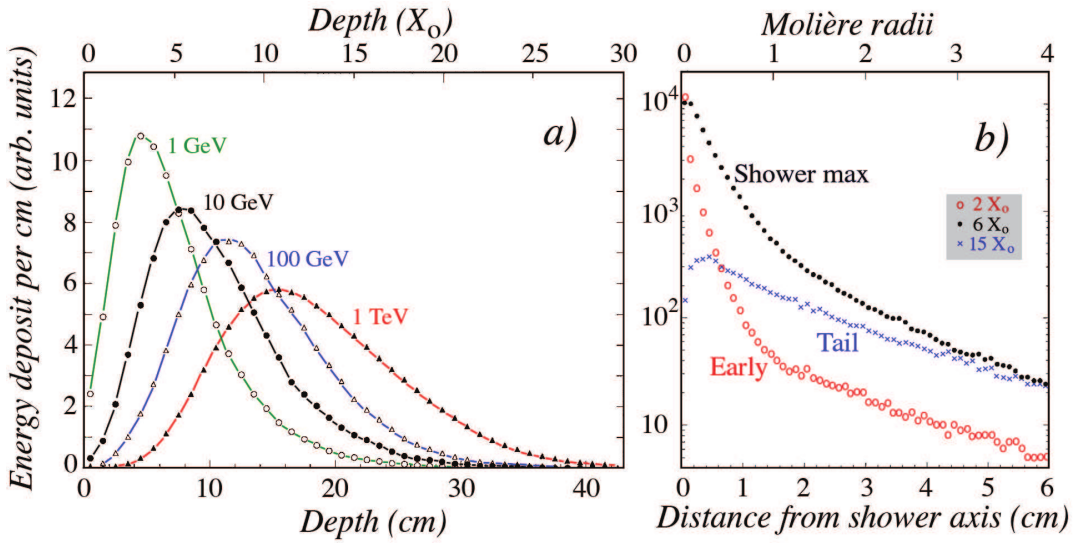


Figure 3.11: Left: the energy deposited as a function of depth for 1, 10, 100 and 1000 GeV electron showers developing in a block of copper; the integral of these curves have been normalized to the same value in order to compare the shower profiles. Right: radial distributions of the energy deposited by 10 GeV electron shower in copper at various depths.

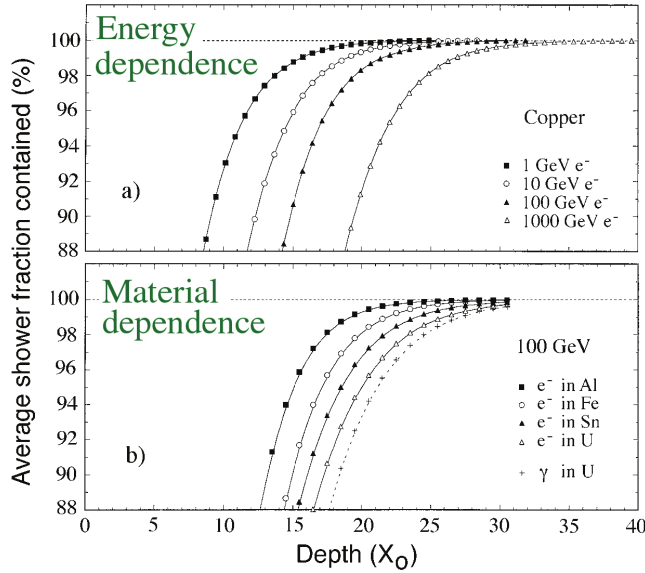


Figure 3.12: Average energy fraction contained in a block of matter with infinite transverse dimensions, as a function of the thickness of the absorber. Up: results for showers induced by electrons of various energies in a copper absorber. Down: results for 100 GeV electron showers in different absorber materials.

On average, hadronic shower profiles look very similar to the electromagnetic ones, except that the scale factor is usually much larger for the hadronic showers. For example, for copper X_0 amounts to 1.4 cm, while $\lambda_{\text{int}} = 15$ cm.

Strong interaction is responsible for:

- The production of hadronic shower particles, of which $\sim 90\%$ are pions. The neutral pions decay in 2γ s, which develop an electromagnetic component in the shower. The fraction of this component depends on the energy of the initial particle.
- The occurrence of nuclear reactions. In these processes, neutrons and protons are released from atomic nuclei, however the nuclear binding energy of these

Effects of strong interactions

nucleons has to be provided. Therefore, the fraction of the shower energy needed for this purpose does not contribute to the calorimeter signals. This is the so called **invisible energy** phenomenon.

So we get in function of the distance travelled inside the calorimeter:

$$N(x) = N_0 e^{-\frac{x}{\lambda_{\text{int}}}} \quad (3.19)$$

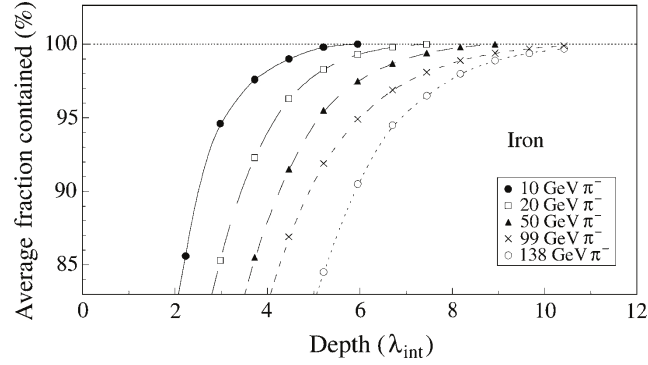


Figure 3.13: Average energy fraction contained in a block of matter with infinite transverse dimensions, as a function of the thickness of the absorber.

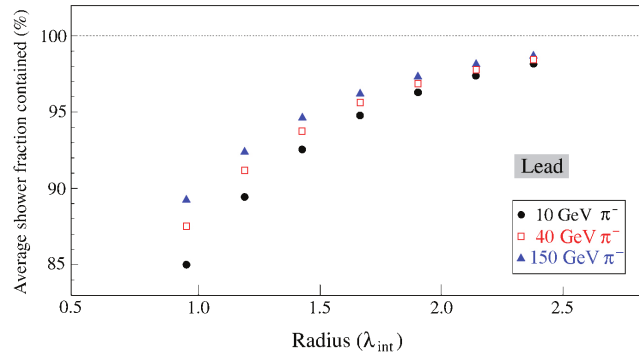


Figure 3.14: Average energy fraction contained in an infinitely long cylinder of absorber material, as a function of the radius of this cylinder, for pions of different energies showering in a lead-based calorimeter.

Consequences of nuclear interaction properties

The large majority of the non-em energy is deposited through nucleons and not through relativistic particles such as pions. These nuclear interaction properties have important consequences for calorimetry:

- As a result of the invisible energy phenomenon, the calorimeter signals for hadrons are in general smaller than for electrons of the same energy.
- Since the electromagnetic energy fraction is energy dependent, the calorimeter is non-linear for hadron detection.

3.4.3 Classification and response of calorimeters

Calorimeters classification

Calorimeters are distinguished according to their composition into two classes:

- **Homogeneous calorimeters**, in which the absorber and the active (signal producing) medium are one and the same. They are used to get high precision results.

- **Sampling calorimeters**, in which these two roles are played by different media. These are layers of active material and high density absorber. This type of calorimeter is more common.

The calorimeter response is defined as the average calorimeter signal per unit of deposited energy. The response is thus expressed in terms of photoelectrons per GeV, pico-coulombs per MeV or something similar. Electromagnetic calorimeters are in general linear, since all the energy carried by the incoming particle is deposited through processes that may generate signals (excitation /ionization of the absorbing medium). Non-linearity is usually an indication of instrumental problems, such as signal saturation or shower leakage. An example of non-linear calorimeter data is given in Figure 3.15.

*Calorimeters
response*

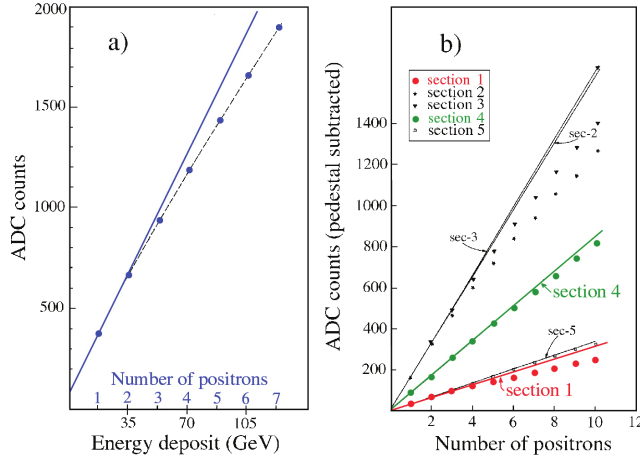


Figure 3.15: Average electromagnetic shower signal from a calorimeter read out with wire chambers operating in the “saturated avalanche” mode, as a function of energy. The calorimeter was longitudinally subdivided.

Calorimeters are based on physical processes that are inherently statistical in nature, so the precision of calorimetric measurements is determined and limited by fluctuations. We examine here the fluctuations that may affect the energy resolution. Many of them will affect electromagnetic and hadronic calorimeters, but the last one has additional term of uncertainty to be discussed later. Fluctuations and contributions to the energy resolution are:

Fluctuations

- Signal quantum fluctuations, such as photoelectron statistics:

$$\frac{\sigma_E}{E} \sim \frac{1}{\sqrt{E}} \quad (3.20)$$

- Shower leakage fluctuations:

$$\frac{\sigma_E}{E} \sim \frac{1}{\sqrt[4]{E}} \quad (3.21)$$

- Fluctuations resulting from instrumental effects, such as electronic noise, light attenuation, structural non-uniformities.

$$\frac{\sigma_E}{E} \sim \frac{1}{E} \quad (3.22)$$

- Sampling fluctuations:

$$\frac{\sigma_E}{E} \sim \text{const} \quad (3.23)$$

So, the calorimeter energy resolution has different contribution from several fluctuation processes, which add in quadrature:

$$\sigma_T^2 = \sigma_1^2 + \sigma_2^2 + \dots + \sigma_n^2 = \sigma_1 \oplus \sigma_2 \oplus \dots \oplus \sigma_n \quad (3.24)$$

For electromagnetic showers, the relevant contributions to the energy resolution can be summarized as:

$$\frac{\sigma}{E} = \frac{a}{\sqrt{E}} \oplus b \oplus \frac{c}{E} \quad (3.25)$$

with a the stochastic term (due to intrinsic shower fluctuations, ...), b the constant term, c the noise term.

For hadronic showers, we have some types of fluctuations as in electromagnetic showers, however, there are some additional effects that tend to dominate the performance of hadron calorimeters.

- Fluctuations in visible energy play a role in all hadron calorimeters and form the ultimate limit to the achievable hadronic energy resolution. So this is an irreducible contribution.
- Fluctuations in the electromagnetic shower fraction causes differences between p and π induced showers since in p showers there are no π^0 .

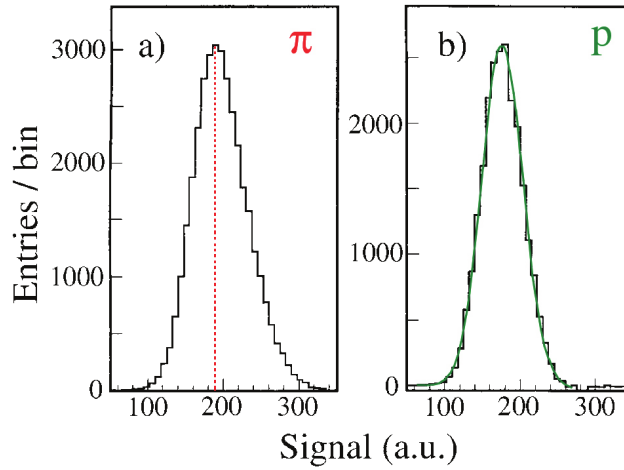


Figure 3.16: Signal distributions for 300 GeV pions and protons detected with a quartz-fiber calorimeter. The curve on the right represents the result of a gaussian fit to the proton distribution.

In the case of hadron calorimeter, the relation used before does not describe the energy resolution due to the two additional effects. For the majority of calorimeters the energy resolution can be approximated by:

$$\frac{\sigma}{E} = \frac{a}{\sqrt{E}} + b \quad (3.26)$$

where a can reach values of 90% and b can be around few %. Therefore, why do we build hadronic calorimeters? In HEP experiments we do not measure single hadrons, we do not reconstruct p , π , etc. We reconstruct jets! Jet reconstruction is complex and

TODO

3.4.4 Particle identification

TODO

Short lived particles are identified through the resonance. Stable or long lived particles are identified exploiting time of flight, Cerenkov, energy loss, combination of tracking and calorimeter.

Chapter 4

Cross section of $e^+e^- \rightarrow \mu^+\mu^-$ and $e^+e^- \rightarrow hh$

The first is a quantum electromagnetic process and it is relatively simple to compute its cross section at first order. It is also our benchmark when we start to study the second process.

Lecture 6.
Wednesday 25th
March, 2020.
Compiled:
Wednesday 15th
April, 2020.

4.1 Muon-Antimuon pair production: $e^+e^- \rightarrow \mu^+\mu^-$

The idea is now to study the cross section of the first process $e^+e^- \rightarrow \mu^+\mu^-$. The matrix elements for this process can be constructed by breaking the process down into components. First, the e^+e^- state is annihilated by an electromagnetic current. This current couples to a quantum state of electromagnetic excitation. Finally, this state couples to another current matrix element describing the creation of the muon pair. These passages can be drawn in a Feynman diagram in a very simple way, as in Figure 4.1.

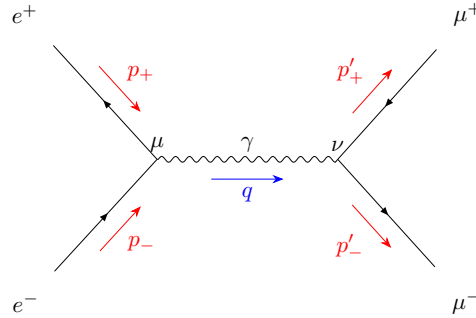


Figure 4.1: Feynman diagram of $e^+e^- \rightarrow \mu^+\mu^-$.

The intermediate photon state can be described as a Breit-Wigner resonance at zero mass. Taking the limit of zero resonance mass in the Breit-Wigner formula, it would then contribute to the scattering amplitude by a factor:

Description as a Breit-Wigner resonance

$$\frac{1}{q^2 - m_R^2 + \frac{i}{2}m_R\Gamma_R} \sim \frac{1}{q^2} \quad (4.1)$$

where q is the momentum carried by the photon from the initial to the final state. Moreover, we consider the reaction at energies large compared to the muon mass and, certainly, very far from the mass shell condition $q^2 = 0$ for a photon, therefore we approximate: $m_e = m_\mu = 0$. A resonance contributing to an elementary particle

Virtual particle
definition and
matrix element

reaction very far from its mass shell is called a **virtual particle**. In this case, we say that the reaction is mediated by a **virtual photon**.

So, the matrix element reads:

$$\mathcal{M}(e^+e^- \rightarrow \mu^+\mu^-) = (-e) \langle \mu^+\mu^- | j^\mu | 0 \rangle \frac{1}{q^2} (-e) \langle 0 | j_\mu | e^+e^- \rangle \quad (4.2)$$

The operator structure $j^\mu j_\mu$ that appears in Eq. 4.2 is called **current-current interaction**.

4.1.1 Properties of massless spin- $\frac{1}{2}$ fermions

We will focus now on the properties of the massless spin- $\frac{1}{2}$ fermions in order to evaluate Eq. 4.2.

Dirac equation in
ultrarelativistic
limit

The dynamics of fermions and the calculation of matrix elements is quite simplified in the ultrarelativistic limit, which is our case since we are considering energies so large that both the electrons and muons are moving relativistically and their masses can be neglected. In this approximation, the Dirac equation takes the form:

$$i\gamma^\mu \partial_\mu \psi = 0 \quad (4.3)$$

where:

$$\gamma^0 = \begin{pmatrix} 0 & \mathbb{1} \\ \mathbb{1} & 0 \end{pmatrix} \quad \gamma^i = \begin{pmatrix} 0 & \sigma_i \\ -\sigma_i & 0 \end{pmatrix} \quad (4.4)$$

It is convenient to write this representation by defining $\sigma^\mu = (\mathbb{1}, \vec{\sigma})^\mu$ and $\bar{\sigma}^\mu = (\mathbb{1}, -\vec{\sigma})^\mu$, so:

$$\gamma^\mu = \begin{pmatrix} 0 & \sigma^\mu \\ \bar{\sigma}^\mu & 0 \end{pmatrix} \quad (4.5)$$

Moreover, we will write $\Psi = (\psi_L, \psi_R)$, so the Dirac equation splits into 2-component equations:

$$i\bar{\sigma} \cdot \partial \psi_L = 0 \quad (4.6a)$$

$$i\sigma \cdot \partial \psi_R = 0 \quad (4.6b)$$

The fields ψ_L and ψ_R annihilate different electron states and create different positron states. These states are not connected by the Dirac equation in this massless limit. When we couple the Dirac equation to electromagnetism, we modify the derivative to include the A_μ field:

Gauge covariant
derivative

$$\partial_\mu \rightarrow D_\mu = (\partial_\mu - ieA_\mu) \quad (4.7)$$

This preserves the separation of the fields ψ_L and ψ_R and of the associated electrons and positrons. The two pieces of the Dirac field communicate only through the mass term. Thus, for zero electron mass or for very high energy where the mass can be neglected, there are essentially two different species of electrons, namely e_L^- and e_R^- . Electromagnetic interactions cannot turn electrons of one kind into the other.

Plane wave
solutions

Now, let's take the equation for ψ_R and let's try to find the plane wave solutions:

$$(i\partial_t + i\vec{\sigma} \cdot \nabla)\psi_R = 0 \implies \psi_R(x) = u_R(p)e^{-iEt+i\vec{p}\cdot\vec{x}} \quad (4.8)$$

where $u_R(p)$ is the 2-component spinor. For simplicity, look for a plane wave moving in the $\hat{z} =: \hat{3}$ direction: $\vec{p} = p\hat{3}$. Then:

$$(E - p\sigma^3)u_R = \begin{pmatrix} E - p & 0 \\ 0 & E + p \end{pmatrix} u_R = 0 \quad (4.9)$$

So, we get two solutions, with the following characteristics:

- $E = p > 0$, $S_3 = \frac{1}{2}$

So the corresponding electron moves at the speed of light and spins in the right-handed sense. The field operator $\psi_R(x)$ destroys an electron in this state.

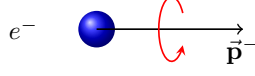


Figure 4.2: Spin up electron.

- $E = -p < 0$, $S_3 = \frac{1}{2}$.

This solution corresponds to the creation of a positron by the Dirac field. The positron has spin down with respect to the direction of motion.

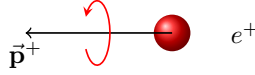


Figure 4.3: Spin down positron.

So we find an electron which is left-handed and a positron which is right-handed¹, and viceversa for the other two solutions of the ψ_L equation, a couple of right-handed electron and left-handed positron.

4.1.2 Matrix element and cross section evaluation

The first step is to evaluate the matrix element for $e_R^-e_L^+$ and $e_L^-e_R^+$ annihilations. In all, the process $e^-e^+ \rightarrow \mu^-\mu^+$ has four amplitudes for the various spin states that are permitted by helicity conservation. All of the differential cross sections have the same structure. So, by considering that:

$$|\mathcal{M}(e_R^-e_L^+ \rightarrow \mu_R^-\mu_L^+)|^2 = |\mathcal{M}(e_L^-e_R^+ \rightarrow \mu_L^-\mu_R^+)|^2 = e^4(1 + \cos\theta)^2 \quad (4.10a)$$

$$|\mathcal{M}(e_R^-e_L^+ \rightarrow \mu_L^-\mu_R^+)|^2 = |\mathcal{M}(e_L^-e_R^+ \rightarrow \mu_R^-\mu_L^+)|^2 = e^4(1 - \cos\theta)^2 \quad (4.10b)$$

we have for example, for $e_R^-e_L^+ \rightarrow \mu_R^-\mu_L^+$:

$$\begin{aligned} \sigma &= \frac{1}{2E \cdot 2E \cdot E} \int d\Pi_2 |\mathcal{M}|^2 \\ &= \frac{1}{2E_{\text{CM}}^2} \frac{1}{8\pi} \int \frac{d\cos\theta}{2} e^4 (1 + \cos\theta)^2 \end{aligned} \quad (4.11)$$

and for $e_R^-e_L^+ \rightarrow \mu_L^-\mu_R^+$:

$$\begin{aligned} \sigma &= \frac{1}{2E \cdot 2E \cdot E} \int d\Pi_2 |\mathcal{M}|^2 \\ &= \frac{1}{2E_{\text{CM}}^2} \frac{1}{8\pi} \int \frac{d\cos\theta}{2} e^4 (1 - \cos\theta)^2 \end{aligned} \quad (4.12)$$

With some algebra, we get the differential cross sections:

*Matrix element
evaluation for the
all possible
annihilations*

*Differential cross
section*

¹We can consider the helicity $h = \hat{p} \cdot \vec{S}$ to describe the solutions. So we get $h = +\frac{1}{2}$ for the left-handed electron and $h = -\frac{1}{2}$ for the right-handed positron.

$$\frac{d\sigma}{d\cos\theta} = \frac{\pi\alpha^2}{2E_{\text{CM}}^2}(1 + \cos\theta)^2 \quad \text{for } e_R^-e_L^+ \rightarrow \mu_R^-\mu_L^+ \text{ and } e_L^-e_R^+ \rightarrow \mu_L^-\mu_R^+ \quad (4.13a)$$

$$\frac{d\sigma}{d\cos\theta} = \frac{\pi\alpha^2}{2E_{\text{CM}}^2}(1 - \cos\theta)^2 \quad \text{for } e_R^-e_L^+ \rightarrow \mu_L^-\mu_R^+ \text{ and } e_L^-e_R^+ \rightarrow \mu_R^-\mu_L^+ \quad (4.13b)$$

Cross section result At the end, we get the final result:

$$\sigma = \frac{4\pi\alpha^2}{3E_{\text{CM}}^2} \quad (4.14)$$

What is important to remember is that the cross section goes as the inverse squared of the energy in the center of mass. This is a common behaviour for electromagnetic interactions. However, at very high energies this behaviour is broken and there are corrections to consider.

How can we measure muons in a given polarization state? Actually, this is very difficult and it is not possible with the odiern technology, so we can measure only in average.

Lecture 7.
Tuesday 31st
March, 2020.
Compiled:
Wednesday 15th
April, 2020.

4.2 Hadron production: $e^+e^- \rightarrow \text{hadrons}$

With the QED process $e^+e^- \rightarrow \mu^+\mu^-$ as a reference point, we can now discuss the process of e^+e^- annihilation to hadrons. The main products of this reaction are observed to be π and K mesons. We will consider the ultrarelativistic regime, so we will consider this process at multi-GeV center of mass energies.

Before beginning with the discussion, we have to remember that hadrons are formed by quarks. Imagine that we are at center of mass energies at which we can ignore the quark masses. Then, since quarks are spin- $\frac{1}{2}$ particles, the structure of the QED cross section for quark pair production is exactly the same as that in the process of muon pair production that we have just analyzed. By stopping here, we are ignoring the effects of the strong interaction, which play an essential role in forming the mesons that appear in the final state. However, this model can be useful as an estimate of the order of magnitude of the cross section or as a reference value.

The changes in the calculations are the following three corrections:

- First, σ depends on E_{CM} , so we must sum over the relevant quark species produced at the given energy. Remember that we can ignore the masses, at the energy we consider, with a good approximation.
- Second, we need to change the value of the electric charge of the produced particles, from -1 for the muon to $Q_f = +\frac{2}{3}$ for u, c , and $Q_f = -\frac{1}{3}$ for d, s, b . The matrix element \mathcal{M} contains one power of the final electric charge, so the cross section is proportional to Q_f^2 .
- Finally, quarks carry a hidden quantum number called color, which can take three values. We need to sum over the final color states in computing the total cross section.

Differential cross section

Thus, these corrections lead to the same angular distribution as before for the muon pair production:

$$\frac{d\sigma}{d\cos\theta} \sim (1 + \cos^2\theta) \quad (4.15)$$

Cross section

while the total cross section is modified to:

$$\sigma(e^+e^- \rightarrow \text{hadrons}) = \sum_f 3Q_f^2 \frac{4\pi}{3} \frac{\alpha^2}{E_{\text{CM}}^2} \quad \text{with } f = u, d, s, c, b \quad (4.16)$$

Note that the quark top t is not included in the sum since its mass is very large and the approximation made before doesn't hold if we include it.

Another quantity that we can analyze is the ratio:

Branching Ratio

$$R = \frac{\sigma(e^+e^- \rightarrow \text{hadrons})}{\sigma(e^+e^- \rightarrow \mu^+\mu^-)} = \sum_f 3Q_f^2 = \begin{cases} 2 & \text{for } u, d, s \\ 3 \cdot \frac{1}{3} & \text{for } u, d, s, c \\ 3 \cdot \frac{2}{3} & \text{for } u, d, s, c, b \end{cases} \quad (4.17)$$

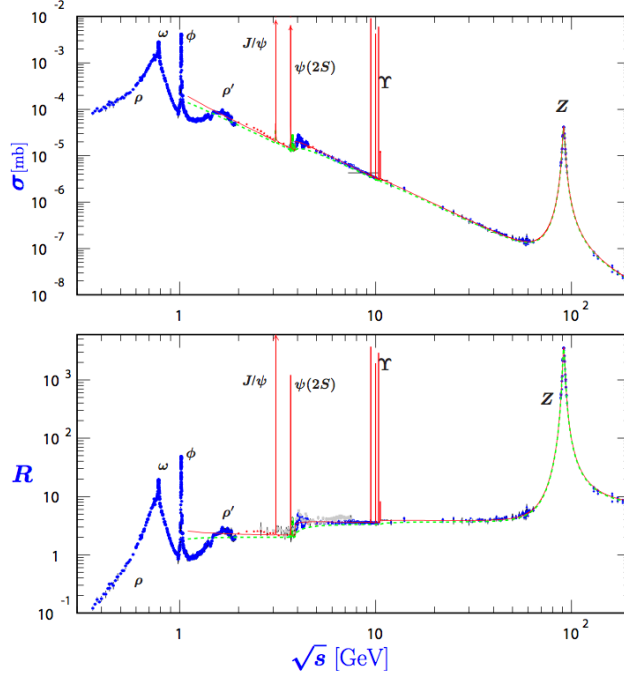


Figure 4.4: Measurements of the total cross section for e^+e^- annihilation to hadrons as a function of energy. The lower figure shows the ratio R . The green dotted curve is the prediction we have found in Eq. 4.17. The vertical lines are the μ resonances, which are very narrow compared to the hadronic ones.

The prediction for the angular distributions can also be tested experimentally. Before considering any method of detailed comparison, we need to ask what $e^+e^- \rightarrow \text{hadrons}$ events actually look like at high energies. Figure 4.5 shows a typical event at $E_{\text{CM}} = 91$ GeV. The tracks are mostly charged pions and kaons. The tracks clearly form two bundles, with π and K mesons moving in opposite directions. We call such a bundle of hadronic tracks a **jet**. The final states of e^+e^- annihilation to hadrons at high energy typically consist of two back-to-back jets.

Definition of jets

Note that quarks are not observed in isolation, but only as constituents of hadrons. However, it is not hard to imagine that a high-energy quark might induce the creation of more quark-antiquark pairs and that all of these might reform into pions and other hadrons. In this understanding, the central axes of the jets would be proxies for the original directions of the quarks. To add some experiment data concerning jet axes, Figure 4.6 shows the orientation of jet axes in e^+e^- annihilation to hadrons at $E_{\text{CM}} = 91$ GeV as a function of $|\cos \theta|$ (and not just $\cos \theta$ since it is difficult to distinguish quark jets from antiquark jets). The functional form is very close to $(1 + \cos^2 \theta)$. The question we'll try to answer is: how is it possible that the strong interactions can be strong and yet these predictions for hadronic processes can be so accurate by neglecting them?

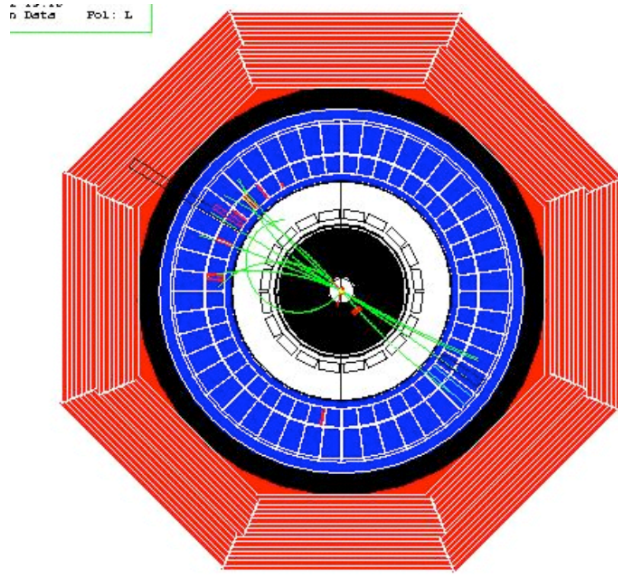


Figure 4.5: Event display from the SLD experiment showing a typical e^+e^- annihilation to hadrons event at a center of mass energy of 91 GeV.

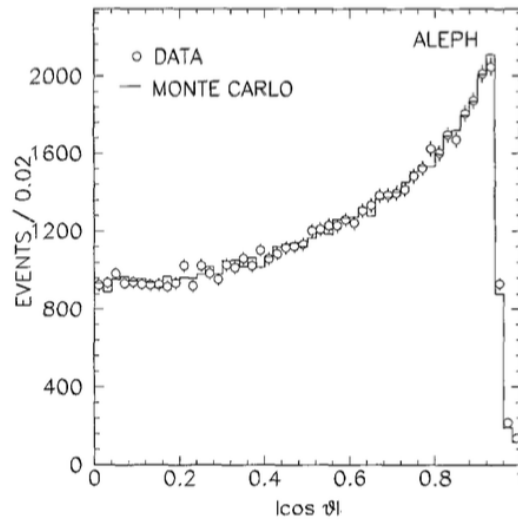


Figure 4.6: Distribution of the orientations of jet axes in e^+e^- annihilation to hadrons as a function of $|\cos \theta|$.

Chapter 5

Deep Inelastic Electron Scattering

The discovery that quarks can be described by spin- $\frac{1}{2}$ particles with simple electromagnetic interactions was actually made, not with this process, but in an earlier experiment studying a reaction in which this conclusion was even more surprising. It is the scattering $e^- p \rightarrow e^- p$.

What we observe in this process is that as the transferred momentum of electron to proton increases, elastic collisions become infrequent. Most scattering events break the proton open and produce a large number of hadrons. When the total mass of the hadrons is much larger than the original proton mass, the reaction is referred to as **deep inelastic electron-proton scattering**. Now we will see that this regime is well described using a picture in which electrons scatter from free quarks inside the proton. What is surprising is that we can ignore the strong interaction to a first approximation in the scattering of the electrons from quarks inside protons.

5.1 The SLAC-MIT experiment

Deep inelastic scattering was first studied in the 1960's at the SLAC linear electron accelerator. The purpose of the experiment was to study the structure of the proton through elastic scattering at high energies. The process can be schematized as follow:

$$e^- p \rightarrow e^- X \quad (5.1)$$

where X can be anything. The electron in the final state goes through a spectrometer in order to reconstruct its 4-momentum. The hadronic final state was ignored.

A Feynman diagram of this process is given in Figure 5.1:

*Feynman diagram
of the process*

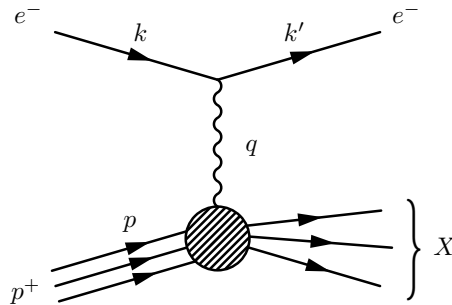


Figure 5.1: Feynman diagram of electron-proton deep inelastic scattering. Source code taken from [4].

The electron interacts with a current matrix element:

$$\langle e^-(k') | j^\mu | e^-(k) \rangle \quad (5.2)$$

The current couples to a virtual photon, which then couples to another current acting on the proton. However, the current matrix element between the proton and the particular hadronic states is not sufficiently simple to exploit for our calculations.

Let's consider k the initial electron momentum and k' the final electron momentum. In the experiment, we prepare k and measure k' , so the momentum of the virtual photon is $q = (k - k')$. Then, the mass W of the final hadronic system is given by:

$$W^2 = (P + q)^2 = m_p^2 + 2P \cdot q + q^2 \quad (5.3)$$

Remember that the energy transfer is much larger than the mass of the proton, so we can ignore both the electron and proton mass. Moreover, q is spacelike, so there exists a frame where the energy transfer is zero and only momentum is transferred. So it is convenient to write $q^2 = -Q^2$.

The cross sections as a function of W for increasing values of $Q^2 = -q^2$ are showed in Figure 5.2. As W increases from left to right in each plot, we see the Δ , N^* , etc., baryon resonances. However, at large Q^2 , the resonances become less visible over a smooth continuum rising with W . This fact shows how complex the data collected were and the challenge of their interpretation.

Mass of the final
hadronic system

Cross section as a
function of W

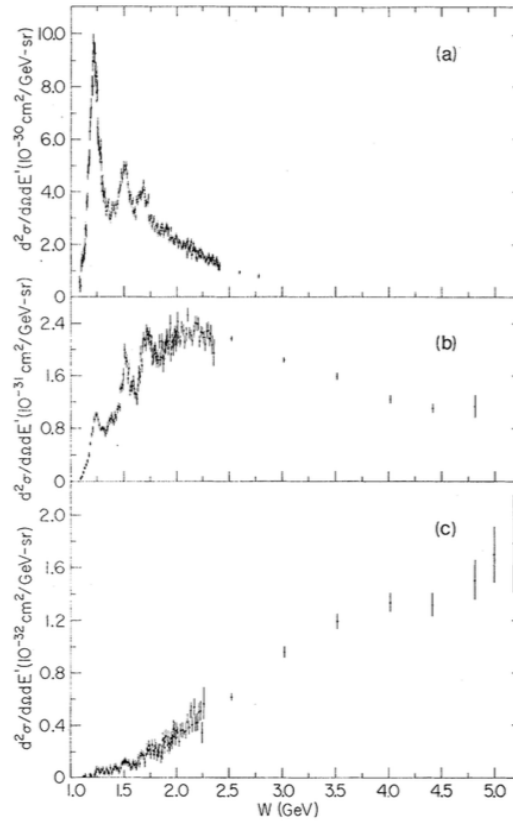


Figure 5.2: Cross section for deep inelastic ep scattering as a function of the final hadronic mass W , measured by the SLAC-MIT experiment, at low, medium, and high values of Q^2 .

5.2 The parton model

To understand the meaning of deep inelastic scattering observed data, Feynman proposed a simple picture based on free quarks and antiquarks that he called **parton**

model. Feynman modeled the proton as a collection of constituents called **partons**. Some of these might be quarks, which we already expect as constituents of the proton. At very high energy, all partons are moving approximately in the direction of the proton, so all partons have a large component of momentum along the direction of the proton, while their transverse momenta remain of the order of the momenta within the proton bound state. So the momentum vector of a parton can be written as:

$$p^\mu = \xi P^\mu \quad (5.4)$$

where P is the total energy momentum of the proton and ξ is the fraction of this energy-momentum carried by that parton. ξ runs over the values 0 and 1.

Let $f_i(\xi)d\xi$ be the probability of finding a parton of type i carrying the momentum fraction ξ . The whole set of partons carry the total energy-momentum of the proton. This implies the sum rule:

$$\int_0^1 d\xi \sum_i f_i(\xi) \cdot \xi = 1 \quad (5.5)$$

In the parton model, deep inelastic scattering is described by the Feynman diagram in Figure 5.3.

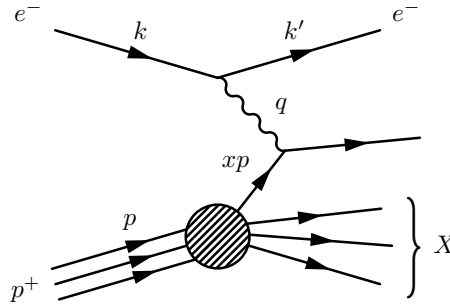


Figure 5.3: Feynman diagram of deep inelastic scattering with a parton.

We take each quark or antiquark in the proton and consider it to scatter from the electron as a pointlike spin- $\frac{1}{2}$ particle. The outgoing quark cannot be seen in isolation since it's not possible to have a quark singlet. Rather, it must turn into a jet of hadrons through processes that involve the strong interactions in a non-trivial way. Here again, the effects of the strong interactions are ignored when computing the cross section, which will be interpreted as the sum of the cross sections for all possible hadronic final states. So, the parton model cross section reads:

$$\sigma(e^- p \rightarrow e^- X) = \int d\xi \sum_f [f_f(\xi) + f_{\bar{f}}(\xi)] \sigma(e^- q(\xi p) \rightarrow e^- q) \quad (5.6)$$

5.3 Crossing symmetry

To compute the cross section, we need to evaluate the matrix elements for electron-quark scattering, which can be described by the Feynman diagram in Figure 5.4.

This diagram is similar to the one for $e^- e^+ \rightarrow \mu^- \mu^+$, so the matrix element will have the same structure:

$$\mathcal{M}(e^- q_f \rightarrow e^- q_f) = (-e) \langle e^- | j^\mu | e^- \rangle \frac{1}{q^2} (Q_f e) \langle q_f | j_\mu | q_f \rangle \quad (5.7)$$

*Definition of
partons*

*Portrait of deep
inelastic scattering
with a parton*

*Cross section for
deep inelastic
scattering
according to
parton model*

Lecture 8.
Wednesday 1st
April, 2020.
Compiled:
Wednesday 15th
April, 2020.

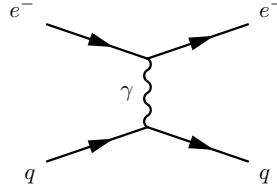


Figure 5.4: Electron-quark scattering Feynman diagram.

To evaluate this matrix element, we need the concept of **crossing symmetry**, applied in a phenomenological way. To begin, we compare the diagram in Figure 5.4 with the following one for $e^+e^- \rightarrow q\bar{q}$ in Figure 5.5.

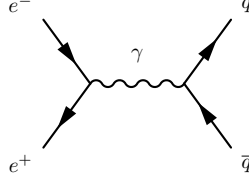


Figure 5.5: Feynman diagram representing quark pair production via electron-positron annihilation.

The two Feynman diagrams actually show the same process, laid out in different ways in space-time. The situations with a final quark and an initial antiquark are strongly related, because the same quantum field that creates the electron destroys the positron, and similarly for a quark and antiquark. So, the matrix elements have the same functional form with appropriate identification of the external momenta.

$$\sum_{\text{spin}} |\mathcal{M}_{\text{scat}}|^2 \longrightarrow \sum_{\text{spin}} |\mathcal{M}_{\text{pair}}|^2 \quad (5.8)$$

Moreover, a theorem from QFT states that processes related by this kind of symmetry are described by the same function of external momenta. It is useful to introduce a rigorous and standard notation for the kinematic invariants of 2-body scattering process. So, we want to study:

$$1(p_1) + 2(p_2) \longrightarrow 3(p_3) + 4(p_4) \quad (5.9)$$

The Mandelstam invariants read (with $p_1^0, p_2^0 < 0$ and $p_3^0, p_4^0 > 0$):

$$s = (p_1 + p_2)^2 = (p_3 + p_4)^2 \quad (5.10a)$$

$$t = (p_1 + p_3)^2 = (p_2 + p_4)^2 \quad (5.10b)$$

$$u = (p_1 + p_4)^2 = (p_2 + p_3)^2 \quad (5.10c)$$

where:

$$s + t + u = m_1^2 + m_2^2 + m_3^2 + m_4^2 \quad (5.11)$$

We write down now the kinematics of the process in the center of mass frame and with the assumption of massless particles, in order to understand better the meaning of s, t, u . The 4-momenta are:

$$p_1 = (-E, 0, 0, -E) \quad (5.12a)$$

$$p_2 = (-E, 0, 0, E) \quad (5.12b)$$

$$p_3 = (E, E \sin \theta, 0, E \cos \theta) \quad (5.12c)$$

$$p_4 = (E, -E \sin \theta, 0, -E \cos \theta) \quad (5.12d)$$

and:

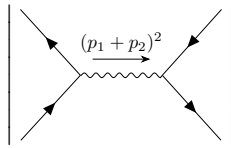
$$s = (2E)^2 = E_{\text{CM}}^2 \quad (5.13)$$

$$t = -2E^2(1 - \cos \theta) \quad (5.14)$$

$$u = -2E^2(1 + \cos \theta) \quad (5.15)$$

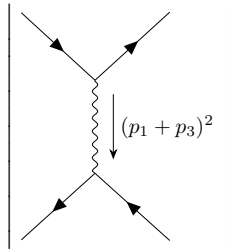
Eqs. 5.13, 5.14, 5.15 are true even for general masses. The two independent variables represented by s, t, u correspond to the CM energy and the CM scattering angle. So s, u, t provide a Lorentz-invariant way to parametrize the two key variables of a scattering process. Concerning the crossing symmetry, an easy way to implement it is to permute the three invariants as the legs of the diagram are switched between the initial and the final state.

In the last chapter, we stated that we could represent an intermediate state in a Feynman diagram with a Breit-Wigner denominator. When the intermediate state separates the initial and the final state, the denominator depends on $(p_1 + p_2)^2 = s$:

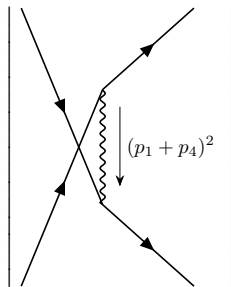


$$\rightarrow \frac{1}{(p_1 + p_2)^2 - m_R^2 + im_R\Gamma_R} = \frac{1}{s - m_R^2 + im_R\Gamma_R} \quad (5.16)$$

This type of reaction is called an ***s*-channel process**. If the amplitude depends on t , we have a ***t*-channel process**, if it depends on u , we have an ***u*-channel process**:



$$\rightarrow \frac{1}{(p_1 + p_3)^2 - m_R^2 + im_R\Gamma_R} = \frac{1}{t - m_R^2 + im_R\Gamma_R} \quad (5.17)$$



$$\rightarrow \frac{1}{(p_1 + p_4)^2 - m_R^2 + im_R\Gamma_R} = \frac{1}{u - m_R^2 + im_R\Gamma_R} \quad (5.18)$$

5.4 Cross section for electron-quark scattering

Crossing symmetry allows us to convert the calculations we did in the previous chapter for e^+e^- annihilation into calculations of the invariant amplitudes for electron-quark scattering. So, by denoting with Q_f the electric charge of the quark in question, we get the following results:

$$|\mathcal{M}(e_R^- e_L^+ \rightarrow q_R \bar{q}_L)|^2 = |\mathcal{M}(e_L^- e_R^+ \rightarrow q_L \bar{q}_R)|^2 = Q_f^2 e^4 (1 + \cos \theta)^2 = 4Q_f^2 e^4 \frac{u^2}{s^2} \quad (5.19)$$

$$|\mathcal{M}(e_R^- e_L^+ \rightarrow q_L \bar{q}_R)|^2 = |\mathcal{M}(e_L^- e_R^+ \rightarrow q_R \bar{q}_L)|^2 = Q_f^2 e^4 (1 - \cos \theta)^2 = 4Q_f^2 e^4 \frac{t^2}{s^2} \quad (5.20)$$

These expressions are correct in any frame and they yield the expressions for the crossed amplitudes after an appropriate permutation of variables. For example, consider the crossing symmetry;

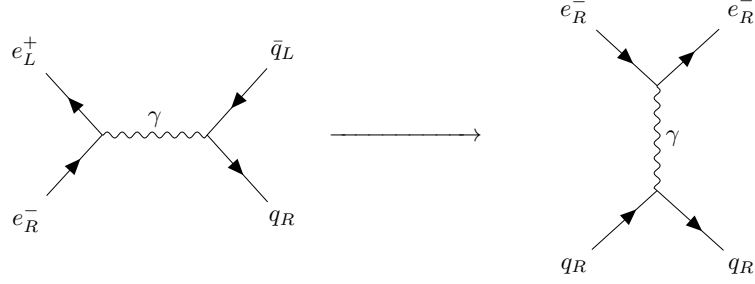


Figure 5.6: Feynman diagram representing the action of crossing symmetry.

The eq scattering diagram on the right of Figure 5.6 is obtained by moving the final antiquark \bar{q}_L to the initial state, where it becomes the quark q_R , and moving the initial positron e_L^+ to the final state, where it becomes the electron e_R^- . Note that helicity is conserved. The interchange of momenta is:

$$\left. \begin{array}{l} p_1 \longrightarrow p_1 \\ p_2 \longrightarrow p_3 \\ p_3 \longrightarrow p_4 \\ p_4 \longrightarrow p_2 \end{array} \right\} \Longrightarrow \left\{ \begin{array}{l} s \longrightarrow t \\ t \longrightarrow u \\ u \longrightarrow s \end{array} \right. \quad (5.21)$$

If we do this exchange, the matrix element for $e_R^- q_R \longrightarrow e_R^- q_R$ is given by:

$$|\mathcal{M}(e_R^- q_R \rightarrow e_R^- q_R)|^2 = 4Q_f^2 e^4 \frac{s^2}{t^2} \quad (5.22)$$

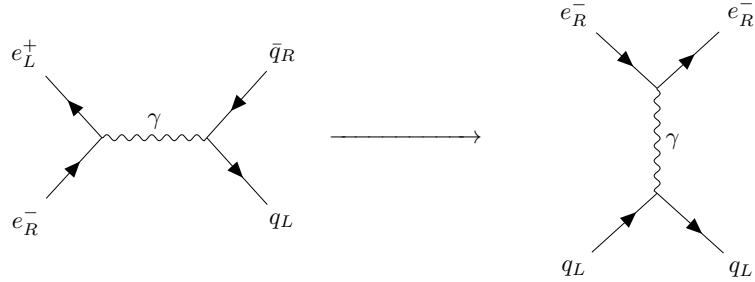


Figure 5.7: Feynman diagram representing the action of crossing symmetry..

Similarly, the crossing symmetry in Figure 5.7 produces:

$$|\mathcal{M}(e_R^- q_L \rightarrow e_R^- q_L)|^2 = 4Q_f^2 e^4 \frac{u^2}{t^2} \quad (5.23)$$

Notice that this matrix element is proportional to $u^2 \sim (1 + \cos \theta)^2$ and vanishes for backward scattering ($\cos \theta = -1$). If we look at the flow of spin angular momentum, we can see that in this case backward scattering is forbidden by angular momentum conservation. The matrix elements for the other helicity combinations allowed by helicity conservation can be obtained in the same way:

$$|\mathcal{M}(e_L^- q_L \rightarrow e_R^- q_L)|^2 = 4Q_f^2 e^4 \frac{s^2}{t^2} \quad (5.24)$$

$$|\mathcal{M}(e_L^- q_R \rightarrow e_R^- q_R)|^2 = 4Q_f^2 e^4 \frac{u^2}{t^2} \quad (5.25)$$

We can now assemble the cross section for eq scattering. Averaging over the spins in the initial state and summing over the spins in the final state, the cross section is given by:

$$\sigma(eq \rightarrow eq) = \frac{1}{2E} \frac{1}{2E} \frac{1}{8\pi} \int \frac{d\cos\theta}{2} \frac{1}{4} \sum_{\text{spins}} |\mathcal{M}(eq \rightarrow eq)|^2 \quad (5.26)$$

There is no color factor of 3 in this equation. Whatever color the quark has in the initial state, that color is passed to the quark in the final state. Summing over the matrix elements for the allowed processes, we find:

$$\frac{d\sigma}{d\cos\theta} = \frac{1}{2s} \pi \alpha^2 \frac{2}{4} \left(4Q_f^2 \frac{s^2 + u^2}{t^2} \right) = \frac{\pi Q_f^2 \alpha^2}{s} \frac{s^2 + u^2}{t^2} \quad (5.27)$$

By changing variable through $dt = \frac{1}{2} s d\cos\theta$, we can rewrite the result completely invariantly:

$$\frac{d\sigma}{dt} = \frac{2\pi Q_f^2 \alpha^2}{s^2} \frac{s^2 + u^2}{t^2} \quad (5.28)$$

Lastly, by combining Eq. 5.6 with Eq. 5.28, we obtain the parton model prediction for deep inelastic scattering cross section:

$$\sigma(e^-p \rightarrow e^-X) = \int d\xi \int d\hat{t} \sum_f [f_f(\xi) + f_{\bar{f}}(\xi)] \frac{2\pi Q_f^2 \alpha^2}{\hat{s}^2} \frac{\hat{s}^2 + \hat{u}^2}{\hat{t}^2} \quad (5.29)$$

The invariants with the hat symbol are used here for the electron-parton scattering process, reserving the symbols without hats for the full electron-proton scattering reaction.

5.5 Bjorken scaling

Let's go further. First of all, $\hat{t} = q^2 = -Q^2$ and this quantity is directly measured in the deep inelastic scattering experiment. Next, we compare s for the full e^-p reaction with \hat{s} for the parton reaction:

$$s = (k + P)^2 = 2k \cdot P \quad (5.30)$$

$$\hat{s} = (k + p)^2 = 2k \cdot p = 2k \cdot \xi P \quad (5.31)$$

So it's evident that $\hat{s} = \xi s$. It is useful to define the quantity y :

$$y = \frac{2P \cdot q}{2P \cdot k} \xrightarrow{\text{proton rest frame}} \frac{q^0}{k^0} \quad (5.32)$$

The physical meaning of y is the fraction of the initial electron energy that is transferred to the proton, so it is bounded between 0 and 1. What we can do now is to express y in function of the Mandelstam invariants for the parton reaction:

$$y = \frac{2\xi P \cdot q}{2\xi P \cdot k} = \frac{2p \cdot (k - k')}{2p \cdot k} = \frac{\hat{s} + \hat{u}}{\hat{s}} \quad (5.33)$$

By reordering, we get:

$$\Rightarrow \frac{\hat{u}}{\hat{s}} = -(1 - y) \quad \text{or} \quad \hat{s}^2 + \hat{u}^2 = \hat{s}^2 [1 + (1 - y)^2] \quad (5.34)$$

Lecture 9.
Tuesday 7th April,
2020.
Compiled:
Wednesday 15th
April, 2020.

All these results should be included in the expression for the cross section $\sigma(e^-p \rightarrow e^-X)$. However, there is one more important kinematic relation to consider. In the parton model, we assumed that the quark is a free point-like Dirac particle and that the electron-quark scattering is elastic. If the final quark is treated as massless particle, then:

$$0 = (p + q)^2 = 2p \cdot q + q^2 = 2\xi P \cdot q - Q^2 \quad (5.35)$$

By reordering Eq. 5.35, we can express the parameter ξ as an observable combination of momenta and we will denote it with x :

$$x = \xi = \frac{Q^2}{2P \cdot q} \quad (5.36)$$

This is a good thing to see since in the parton model a deep inelastic scatter at a fixed value of x is due to an initial parton carrying the fraction x of the initial proton momentum. By measuring x , we can sample the momentum distributions of quarks in the proton wavefunction. By combining the previous results:

$$Q^2 = xys \quad (5.37)$$

and with x fixed:

$$d\hat{t} = dQ^2 = xsdy \quad (5.38)$$

This gives our final formula for the deep inelastic scattering cross section:

$$\frac{d\sigma}{dx dy}(e^-p \rightarrow e^-X) = \sum_f xQ_f^2 [f_f(x)f_{\bar{f}}(x)] \cdot \frac{2\pi\alpha^2 s}{Q^4} [1 + (1-y)^2] \quad (5.39)$$

with $0 < x, y < 1$.

We can rewrite this result by introducing a **form factor** F_2 , which contains the information about the proton structure and it is unknown:

$$\frac{d\sigma}{dx dy}(e^-p \rightarrow e^-X) = F_2 \cdot \frac{2\pi\alpha^2 s}{Q^4} [1 + (1-y)^2] \quad (5.40)$$

F_2 could depend on the general kinematics of the problem, so it could be a general function of x and Q^2 :

$$F_2(x) = \sum_f xQ_f^2 [f_f(x)f_{\bar{f}}(x)] \quad (5.41)$$

What is surprising is that the predicted form depends only on x and it is independent of Q^2 . This behaviour is called **Bjorken scaling**, from the name of the physicist who predicted this simple dependence based on more advanced hypotheses about the behaviour of current matrix elements at high energy. An example of the described behaviour is showed in Figure 5.8, where all of the data falls on a single curve as a function of x .

Over the past decades, F_2 has been measured repeatedly at higher energies, using muons and neutrinos produced by proton beams of hundreds of GeV. The full world data set, collected by the Particle Data Group is showed in Figure 5.9.

In conclusion, we saw that e^-p deep inelastic scattering allows us to measure a quantity $F_2(x)$, interpreted as a sum over parton distributions for quarks and antiquarks in the proton, and where x is the fraction of the momentum of a proton carried by a quark and $f_f(x)$, $f_{\bar{f}}(x)$ are the parton distribution functions. In particular, these ones are the probability distribution of quarks and antiquarks of flavor f in the proton as a function of x .

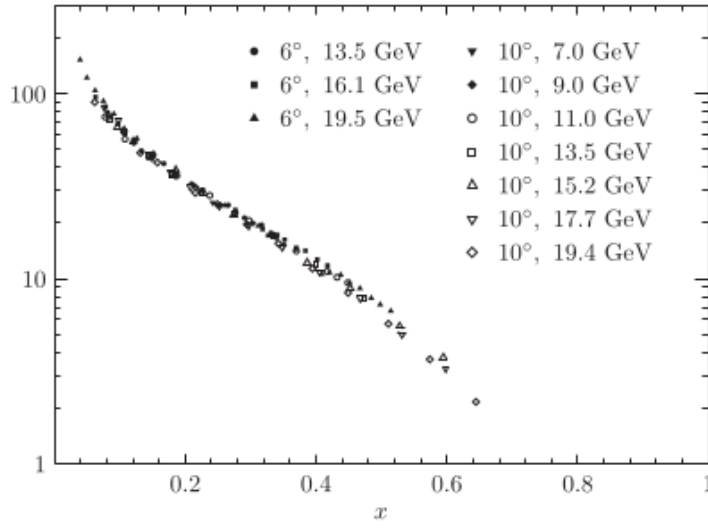


Figure 5.8: Measurements of the quantity F_2 by the SLAC-MIT experiment, at energy and angle settings giving $Q^2 > 1 \text{ GeV}^2$, plotted as a function of x .

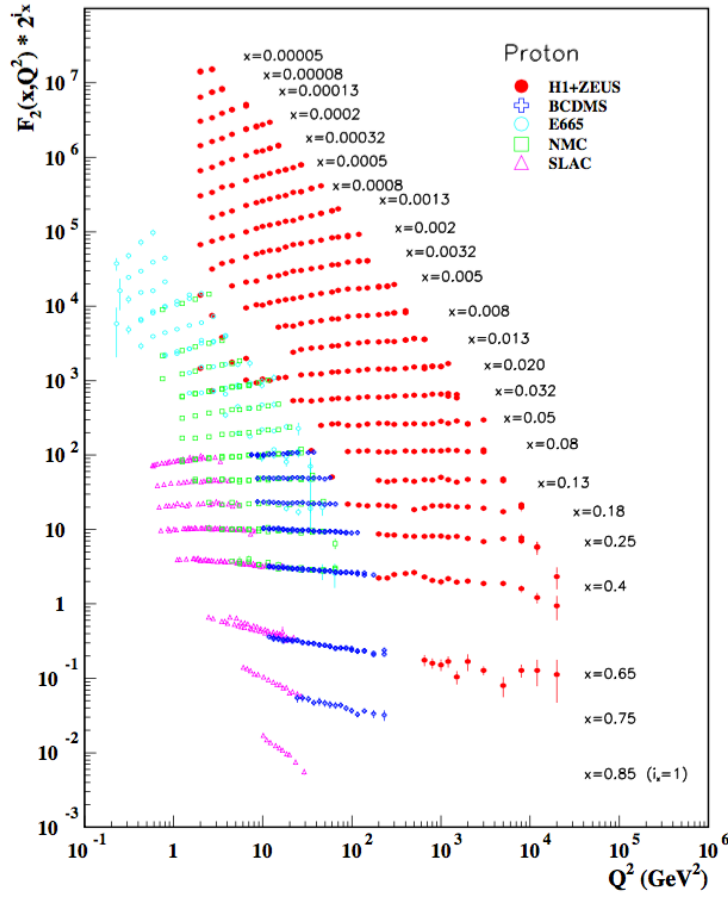


Figure 5.9: Measurements of the quantity F_2 at increasing values of x as a function of Q^2 , compiled by the Particle Data Group.

Chapter 6

Strong interactions

6.1 The gluon

6.1.1 Measurement of parton distribution functions

Let's begin by returning on the final discussion in the previous chapter. We want to know the probability density functions (PDFs) at high energies. In order to understand their utility, we take the example of the proton, composed of three quarks, in particular uud . However in its $F_2^p(x)$ factor we can have contributions from other quarks and not only by u and d . However, there are certain rules that should be satisfied:

$$\int_0^1 dx [f_u(x) - f_{\bar{u}}(x)] = 2 \quad (6.1)$$

$$\int_0^1 dx [f_d(x) - f_{\bar{d}}(x)] = 1 \quad (6.2)$$

$$\int_0^1 dx [f_q(x) - f_{\bar{q}}(x)] = 0 \quad q = s, c, b, t \quad (6.3)$$

These PDFs have to be measured experimentally, in our case the reaction $e^-p \rightarrow e^-X$ gives us one combination of these distributions. But there are other reactions that give us access to other, orthogonal, combinations.

Another important source of information is deep inelastic scattering by neutrinos. Neutrinos interact with protons through the weak interaction, and so we will need to understand the structure of that interaction to interpret this data in detail. We will see later that neutrinos also interact through a form of the current-current interaction, and that, at the level of the parton model, neutrino and antineutrino deep inelastic scattering is also described by a formula similar to the one we found. The four most important parton-level processes are:

$$\nu + d \rightarrow u + \mu^- \quad (6.4)$$

$$\nu + \bar{u} \rightarrow \bar{d} + \mu^- \quad (6.5)$$

$$\bar{\nu} + u \rightarrow d + \mu^+ \quad (6.6)$$

$$\bar{\nu} + \bar{d} \rightarrow \bar{u} + \mu^+ \quad (6.7)$$

$$(6.8)$$

To measure the cross section of electron-proton interaction, we can measure something similar with muons. So we are looking to processes with a muon in the final state. By measuring the sign of the final muon each event and the distribution of events in y , we can separately measure u and d quark and antiquark distributions. By looking for strange or charmed particles in the final states of deep inelastic electron and neutrino

Lecture 10.
Wednesday 8th
April, 2020.
Compiled:
Wednesday 15th
April, 2020.

*Flavor sum rules
for PDFs*

scattering, we can also estimate the heavy quark distributions. Note that the sum rules imply that the total numbers of heavy quarks and antiquarks in the proton are equal, but they do not imply that $f_f(x) = f_{\bar{f}}(x)$. In fact, some processes that add quark-antiquark pairs lead to different distributions.

Using data from all of these reactions, it is possible to assemble a quantitative model of the full set of pdfs. In setting up such a model, we typically divide the u and d pdfs into **valence** and **sea components**. The valence component contains exactly two u quarks and one d quark, at values of x of order 1. These distributions will have the general form in Figure 6.1. These valence quarks are accompanied by a sea of quarks and antiquarks. The sea distributions are largest at much smaller values of x . They are found to be divergent as x approaches to 0, so that the proton contains a very large number of quark-antiquark pairs carrying very small fractions of the total proton momentum. This can be seen in Figure 6.2.

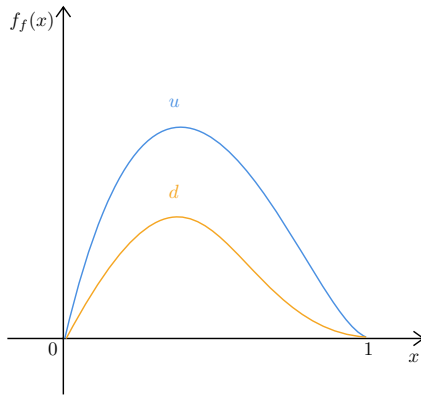


Figure 6.1: The pdfs of the proton: valence components.

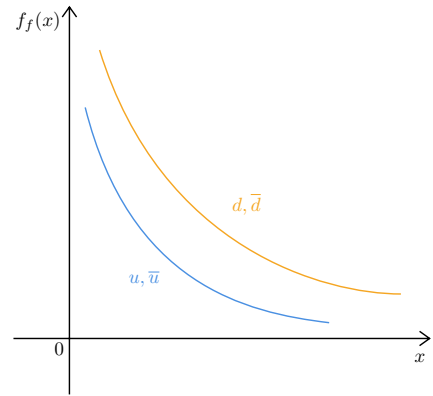


Figure 6.2: The pdfs of the proton: sea components.

The divergences of the quark and antiquark pdfs must match so that the integrals in the sum rules can be finite. Feynman called the partons at very small x the **wee partons**.

These ideas can be incorporated in a quantitative model of the pdfs whose parameters are then fit to the relevant data. The fit gives explicit forms for the valence and sea pdf functions. Figure 6.3 shows the functions extracted by the NNPDF collaboration. Now, since each parton carries a fraction x of the proton's energy-momentum:

$$\int dx \, x \sum_i f_i(x) = 1 \quad (6.9)$$

The fraction of the total energy-momentum of the proton carried by quarks is given by the integral:

$$\frac{P_{q+\bar{q}}}{P} = \int_0^1 dx \, x \sum_f [f_f(x) + f_{\bar{f}}(x)] \approx 0.5 \quad (6.10)$$

With the extra factor of x , this integral easily converges as x approaches 0. So, something is still missing since we expect $\frac{P_{q+\bar{q}}}{P} \approx 0.5$. We need additional partons of another type and it shouldn't participate in deep inelastic scattering. Presumably, the proton must also contain the particle responsible for the binding of quarks into hadron bound states. This particle is called **gluon**. If gluons lead to the strong interaction, then, also, there should be a field equation for the gluon field, and there should be

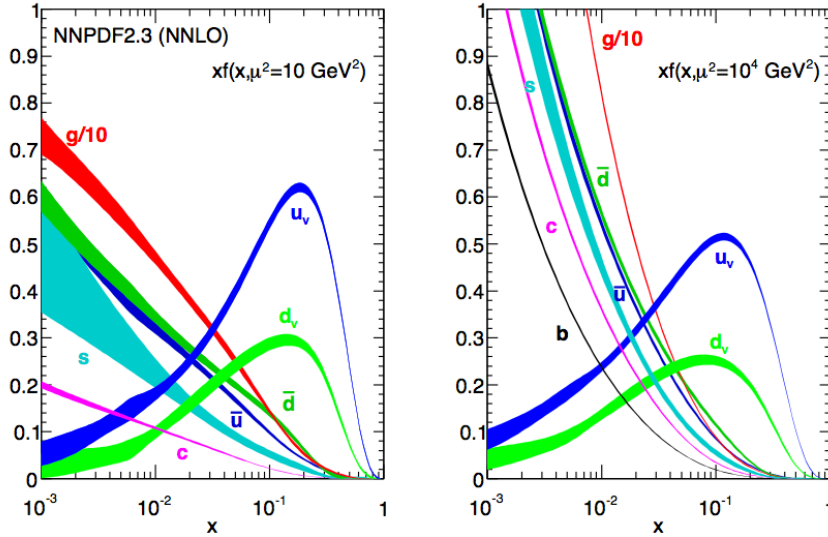


Figure 6.3: Parton distribution functions $xf_i(x)$ at $Q = 3.1$ GeV and at $Q = 100$ GeV, according to the fit of the NNPDF collaboration.

physical gluon particles. These particles should appear in the proton wavefunction and should carry some fraction of its momentum. The gluon should be radiated from the outgoing quarks and antiquarks.

If there is a gluon that interacts with quarks, it should be produced in the reaction $e^+e^- \rightarrow \text{hadrons}$. We have seen that typical events for this process at high energies are 2-jet events, due to quarks and antiquarks. If a gluon also appears as a jet, we should also see 3-jet events, in which one jet is the product of a gluon. And this is what was observed experimentally.

6.1.2 Photon emission in $e^+e^- \rightarrow q\bar{q}$

Let's start by formulating a hypothesis. The simplest one is that gluons are spin 1 particles like photons, and that they couple to the conserved quark current in the same manner as the photon. The theory of photon emission from relativistic charged particles is rather straight-forward.

We focus now on the process of e^+e^- annihilation into hadrons. The final state of two collinear particles has a momentum very close to that of the original particle, so only a small momentum transfer is required. This process is called **collinear splitting**. In particle detectors, splitting is induced by the interaction of the electron or photon with an atomic nucleus. However, when a relativistic particle is produced in a hard-scattering reaction, that reaction can give the small amount of extra momentum needed to allow splitting.

Consider, then, Feynman diagram with $e^+e^- \rightarrow q\bar{q}$ followed by photon:

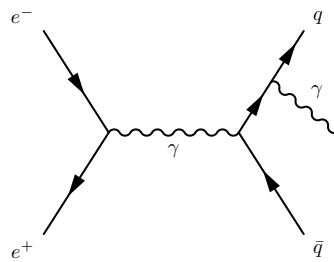


Figure 6.4: Feynman diagram of $e^+e^- \rightarrow q\bar{q}$ followed by photon.

In the full process $e^+e^- \rightarrow q\bar{q} + \gamma$, photons can also be emitted from the initial-state electron and positron, and all of these emissions must be accounted to compare with data. However, it turns out that the dominant contribution to the cross section consists of separate contributions from each of the initial and final legs, so it makes sense to study these separately.

We can study the gluon emission in e^+e^- interaction:

- $e^+e^- \rightarrow q\bar{q}g \rightarrow 3 \text{ jets}$
- $e^+e^- \rightarrow q\bar{q} \rightarrow q\bar{q}g$

6.1.3 Gluon effects on PDFs

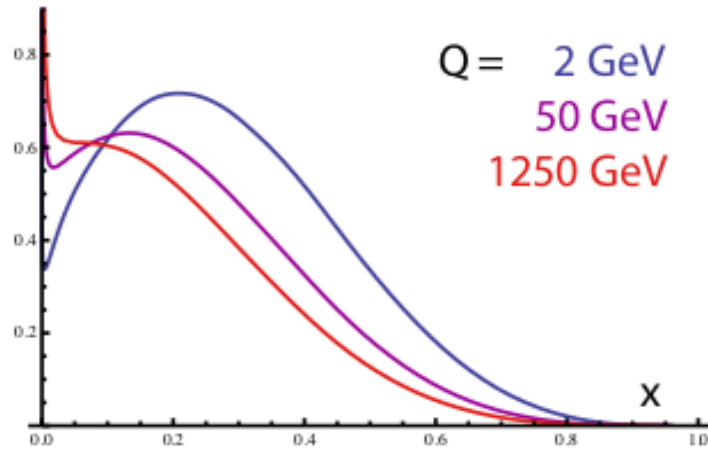


Figure 6.5: Evolution of the u quark pdf $xf_u(x)$ from $Q = 2$ GeV to $Q = 1250$ GeV, showing the flow of valence quark energy-momentum into gluons.

Chapter 7

Exercises

Exercise 1

Calculate the average number of particles in an electromagnetic shower initiated by a 50 GeV photon, after 10, 13 and 20 cm of crossed iron.

Hint: search for the radiation length of the iron on the PDG.

Searching on Particle Data Group^a, we find for e^- :

$$X_0^{\text{Fe}} = 1.757 \text{ cm} \quad (7.1)$$

$$E_C^{\text{Fe}} = 21.68 \text{ MeV} \quad (7.2)$$

So, until the energy of the product particles is lower than the critical energy E_C , we have:

$$N(x) = 2^{\frac{x}{X_0^{\text{Fe}}}} \quad (7.3)$$

We find these values:

$$N(x = 10 \text{ cm}) \approx 52 \quad (7.4)$$

$$N(x = 13 \text{ cm}) \approx 169 \quad (7.5)$$

$$N(x = 20 \text{ cm}) \approx N(x \approx 19.6 \text{ cm}) \approx 2306 \quad (7.6)$$

We note that for $x = 20 \text{ cm}$, the critical energy has already been reached at $x \approx 19.6 \text{ cm}$, so the number of product particles has to be computed at this distance with Eq. 7.3.

^ahttp://pdg.lbl.gov/2010/AtomicNuclearProperties/HTML_PAGES/026.html

Exercise 2

A muon of 100 GeV energy crosses without being absorbed a detector whose mass is mainly due to the hadronic calorimeter and to the muon detector. The thickness of the crossed material can be considered as a layer of 3 m of iron. Determine:

- What is the dominant energy loss process.
- The average loss of the muon inside the detector.

Hint: look at the energy loss picture of muons.

Bibliography

- [1] Michael E. Peskin *Concepts of Elementary Particle Physics*. Oxford Master Series in Particle Physics, Astrophysics and Cosmology April 2, 2019
- [2] Richard Wigmans Department of Physics, Texas Tech University, Lubbock, TX 79409-1051, U.S.A. *Calorimetry*. http://siba.unipv.it/fisica/ScientificaActa/volume_2_1/Wigmans.pdf
- [3] C. W. Fabjan (CERN, Geneva, Switzerland) and T. Ludlam (Brookhaven National Laboratory, Upton, Long Island, New York 11973, USA) *Calorimetry in high-energy physics*. <https://www.annualreviews.org/doi/pdf/10.1146/annurev.ns.32.120182.002003>
- [4] <https://wiki.physik.uzh.ch/cms/latex:feynman>